

Received August 9, 2019, accepted September 23, 2019, date of current version October 17, 2019.

Digital Object Identifier 10.1109/ACCESS.2019.2945501

# Tracking Control With Input Saturation and Full-State Constraints for Surface Vessels

YUANHUI WANG<sup>1</sup>, XIYUN JIANG, WENCHAO SHE, AND FUGUANG DING

College of Automation, Harbin Engineering University, Harbin 150001, China

Corresponding author: Fuguang Ding (dingfuguang@hrbeu.edu.cn)

This work was supported in part by the National Nature Science Foundation of China, under Grant 51879049, and in part by the Natural Science Foundation of Heilongjiang Province, China, under Grant LH2019E039.

**ABSTRACT** To solve the problems of full-state constraints in trajectory tracking of surface vessels, a backstepping technique combining a novel integral barrier Lyapunov function (iBLF) with neural network and sliding mode is proposed. Moreover, the control law is extended to the control problem with input saturation. First, the iBLF-based control approach is applied to the control design. The purpose of the iBLF-based approach is to deal with the constraints without transforming the constraints bound into the tracking errors bound. Second, the Neural Networks (NN) is used to handle with the system uncertainties, and a single parameter online adjustment is used instead of the weights online adjustment of the neural networks to realize the adaptive estimation of a single parameter. Third, defining an auxiliary analysis system to deal with the effect of input saturation on the system, an effective control approach under input saturation is realized. Furthermore, it is proved that the designed control law can guarantee the uniformly ultimately bounded stability of closed-loop system and system state can not violate the constraints. Finally, the simulation results of trajectory tracking control of the surface vessel show that the proposed control approach can effectively solve the control problem of nonlinear systems with full-state constraints, system uncertainties and input saturation.

**INDEX TERMS** Surface vessels, backstepping, full-state constraints, input saturation, neural network.

## I. INTRODUCTION

In recent years, with the increasing needs of the marine engineering [1], the higher accuracy of the trajectory tracking control of surface vessels for different mission requirements is strongly needed. Research on the nonlinear control approaches for surface vessels have become a hot topic [2]–[5]. State constraints is a challenge in trajectory tracking of surface vessels. Once the system violates the constraints during the operation, the system dynamic performance degradation may occur, and it is difficult to meet the control requirements. In order to stabilize the system under the constraints, artificial potential field [6], [7], model predictive control [8], [9] and invariant set [10], [11] are applied. Compared to these approaches, the barrier Lyapunov function (BLF) approach is used to handle the system constraints by Lyapunov-based control design technique, which averts the need for explicit solutions. Ren *et al.* [12] proposed a class of constraint control approach based on BLFs. By constructing the explicit BLFs, the controller for con-

strained control system can be designed by combining Lyapunov direct method with other mature control approaches. Tee *et al.* [13], [14] used the BLFs to solve nonlinear system control problems with constraints. Ren *et al.* [15] applied the BLF control approach to the control design of nonlinear systems with state constraints. However, most of the references using BLF-based approaches adopt a log-type BLF to deal with the state constraints of nonlinear systems. This approach converts actual constraints into system tracking error constraints for indirect processing rather than directly dealing with actual constraint problems. In view of this situation, Tang *et al.* [16] applied the integral barrier Lyapunov functions (iBLFs) to deal directly with a class of perturbed uncertain nonlinear systems with full-state constraints. Furthermore, Tang *et al.* [17] presented an iBLF control scheme to the control design of an uncertain robotic manipulator with joint space constraints. Li *et al.* [18] applied the iBLF directly to deal with the nonlinear systems with uncertain parameters and full-state constraints. To highlight the effectiveness of the BLFs approach, in recent years, some scholars have applied this approach to the trajectory tracking control problem of the surface vessels to effectively solve the output

The associate editor coordinating the review of this manuscript and approving it for publication was Haiyong Zheng<sup>1</sup>.

constraints and full-state constraints in the control process. Zhao *et al.* [19] combined the log-type BLF with the Neural Networks to design the controller for uncertain multiple-input and multiple-output (MIMO) surface vessel with output constraints. Based on the same approach, Yin *et al.* [20] completed the control design for the MIMO surface vessel with full-state constraints and uncertain parameters. Few iBLF approaches are used to solve the trajectory tracking control problem for surface vessels with full-state constraints. Therefore, it is of novelty to handle trajectory tracking problem in the control design process for the surface vessels.

In the aforementioned control designs using BLFs, the input saturation of actual system are hardly considered. Input saturation is a potential problem for systems since the control input calculated by the controller may exceed the maximum that the system control input can produce. This would give rise to degraded performance and even instability of the nonlinear systems. In the presence of input saturation, Wen *et al.* [21] designed an adaptive control law for uncertain nonlinear systems under external disturbance and asymmetric saturation, where input saturation was handled by using a smooth function. Wang *et al.* [22] proposed a robust adaptive fuzzy control algorithm for pure-feedback stochastic nonlinear systems with input saturation. A piecewise smooth function is introduced to approximate the saturation function. Veksler *et al.* [23] developed model predictive control (MPC) for the dynamic positioning systems combining control design with allocation. They applied the optimization problem of MPC to handle actuator saturation. Perez and Donaire [24] presented a passivity-based control scheme for dynamic positioning system, where input saturation was handled by using the anti-windup compensator. Chen *et al.* [25] proposed a robust adaptive neural network control approach for MIMO nonlinear systems with input saturation. The auxiliary design system was introduced to analyze the influence of input constraints. Du *et al.* [26] designed robust controllers for dynamic positioning vessels with external disturbances and input saturation and introduced auxiliary dynamic systems to solve input saturation problem. The approaches proposed in the above references effectively solve the system input saturation problem, but they all neglect state constraints that exist in the actual system. Therefore, it is necessary to solve the problem of input saturation and state constraints simultaneously.

Moreover, vessels may unstable without close-loop control, especially in transit while withstanding waves, currents and wind. Fossen and Grovlen *et al.* [27] designed dynamic positioning control law by using backstepping approach, where disturbances including waves, currents and wind were neglected. In addition, the vessels dynamics are highly nonlinear and contain unknown parametric or functional uncertainties. If these factors are not taken into consideration, this may lead to degraded performance or even instability. In the presence of the system uncertainties, He *et al.* [28], [29] proposed a boundary control approach for a flexible marine riser. Yang *et al.* [30] constructed a class of disturbance

observers to approximate external disturbances of the surface vessels. Ghommam *et al.* [31] used Lyapunov direct method and backstepping technique to design a class of surface vessel path tracking controller, where the unmeasured state of the system was solved by nonlinear state observer. Yu *et al.* [32] proposed a sliding mode controller for surface vessels. However, all these approaches need to be based on accurate mathematical models. Compared with other approaches, in the field of control engineering, neural networks (NN) is one of the most effective method to deal with system uncertainties. With the help of NN approximation, it is not necessary to spend much effort on system modeling in case such modeling processes are always highly difficulty and time consuming. For example, backstepping technique and adaptive neural control are used to solve the control problem of a class of uncertain nonlinear systems [33]–[36]. The sliding mode approach was combined with neural network in backstepping design for uncertain nonlinear systems [37]–[39]. Although the above references use neural networks to deal with system uncertainties, the disadvantage is that once the number of network nodes increases, the adaptive parameters will increase, which is not conducive to real-time control. Therefore, we utilize a NN minimum parameter learning technique to overcome above defects.

This paper investigates trajectory tracking control for surface vessels with full-state constraints, uncertainties and input saturation. The main contributions of this paper are summarized as follows:

- 1) Compared with [20], a novel iBLF is employed for MIMO surface vessel full-state constraints control design to deal with constraints directly, without converting constraints into upper bounds of tracking errors. In addition, the full-state constraints approach based on iBLF is extended to the study of input saturation approach.
- 2) The uncertainties of the surface vessels are approximated by RBF neural network. Compared with [19], the ideal weight matrix estimation of the neural network is converted into a single parameter estimation, which reduces the adjustment of adaptive parameters and accelerate the solving process of adaptive law.
- 3) [19] and [20] consider the output and state constraints for surface vessels, but they did not consider the physical constraints of the system actuators. Therefore, we adopt a dynamic auxiliary analysis system to prevent actuators input signal saturation.
- 4) It is proven that all signals in this closed-loop system are bounded according to Lyapunov method.

The organization of this paper is as follows. In Section II, the problem formulation and preliminaries are given. In Section III, a iBLF-based backstepping control design combined with neural network sliding mode approach is proposed for the surface vessels with state constraints, input saturation and uncertainties. The closed-loop system stability is analyzed as well. In Section IV, the simulation

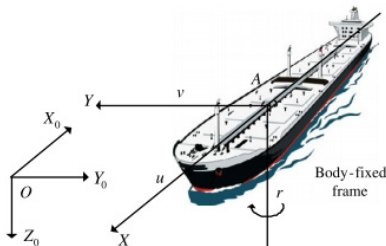


FIGURE 1. Frames and states of the surface vessel.

studies demonstrate the effectiveness of the approach. The last section concludes the work in this paper.

## II. PROBLEM FORMULATION AND PRELIMINARIES

### A. PROBLEM FORMULATION

A surface vessel in the horizontal plane is shown in Fig. 1 [26]. The origin  $O$  of inertial frame  $O-X_0Y_0Z_0$  is fixed to the Earth, and can be chosen as any point on the earth's surface. The  $OX_0$  axis and the  $OY_0$  axis point to north and east, respectively.  $OZ_0$  axis points towards the center of the earth. The body-fixed frame  $A-XYZ$  is a moving coordinate frame which is fixed to the surface vessel. The origin  $A$  of the body-fixed frame is located at the gravity center of the surface vessel. The  $AX$  axis points to the head of the surface vessel. The  $AY$  axis points to right and is perpendicular to  $AX$  axis, and  $AZ$  axis is perpendicular to the plane of  $XAY$ . Then the three-degrees-of-freedom motion of surface vessel vectorial model is

$$\begin{aligned} \dot{\eta} &= \mathbf{R}(\psi)\mathbf{v} \\ \mathbf{M}\dot{\mathbf{v}} + \mathbf{C}(\mathbf{v})\mathbf{v} + \mathbf{D}(\mathbf{v})\mathbf{v} &= \boldsymbol{\tau} + \mathbf{d}(t) \end{aligned} \quad (1)$$

where  $\eta = [x, y, \psi]^T \in \mathbb{R}^3$ ; in the earth-fixed frame  $x, y$  and  $\psi$  are the position and the heading angle, respectively;  $\mathbf{v} = [u, v, r]^T \in \mathbb{R}^3$ ,  $u, v$  and  $r$  are surge, sway, and yaw velocities, respectively;  $\mathbf{R}(\psi)$  is the rotation matrix given by

$$\mathbf{R}(\psi) = \begin{bmatrix} \cos \psi & -\sin \psi & 0 \\ \sin \psi & \cos \psi & 0 \\ 0 & 0 & 1 \end{bmatrix} \quad (2)$$

$\mathbf{M} \in \mathbb{R}^{3 \times 3}$  is the unknown symmetric positive inertia matrix;  $\mathbf{C}(\mathbf{v}) \in \mathbb{R}^{3 \times 3}$  is the unknown centripetal and Coriolis torques matrix;  $\mathbf{D}(\mathbf{v}) \in \mathbb{R}^{3 \times 3}$  is the unknown hydrodynamic damping matrix.  $\boldsymbol{\tau} = [\tau_1, \tau_2, \tau_3]^T$  is the control vector produced by the propulsion system, consisting of control forces  $\tau_1$  in surge,  $\tau_2$  in sway and moment  $\tau_3$  in yaw. Due to the physical constraints of actuators can be described as follows.

$$\tau_i = \begin{cases} \tau_{imax}, & \tau_{ci} > \tau_{imax} \\ \tau_{ci}, & \tau_{imin} \leq \tau_{ci} \leq \tau_{imax} \\ \tau_{imin}, & \tau_{ci} < \tau_{imin} \end{cases} \quad i = 1, 2, 3 \quad (3)$$

where  $\tau_{imax}$  and  $\tau_{imin}$  are the maximum and the minimum generalized control forces that the surface vessel's propulsion system can produce, respectively.  $\boldsymbol{\tau}_c = [\tau_{c1}, \tau_{c2}, \tau_{c3}]^T$  is the control vector in surge, sway and yaw.

$\mathbf{d}(t) = [d_1(t), d_2(t), d_3(t)]^T$  denotes the disturbance vector in surge, sway and yaw.

For convenience, let  $\mathbf{x}_1 = \eta$ ,  $\mathbf{x}_2 = \mathbf{v}$ , then (1) can be described as

$$\begin{aligned} \dot{\mathbf{x}}_1 &= \mathbf{R}(\mathbf{x}_1)\mathbf{x}_2 \\ \dot{\mathbf{x}}_2 &= \mathbf{M}^{-1}[-\mathbf{C}(\mathbf{x}_2)\mathbf{x}_2 - \mathbf{D}(\mathbf{x}_2)\mathbf{x}_2 + \boldsymbol{\tau} + \mathbf{d}(t)] \end{aligned} \quad (4)$$

where  $\mathbf{x}_1 = [x_{11}, x_{12}, x_{13}]^T$ ,  $\mathbf{x}_2 = [x_{21}, x_{22}, x_{23}]^T$ .

The two main aspects of control objectives are as follows:

1) The system state  $\mathbf{x}_1(t)$  can tracks the desired trajectory  $\boldsymbol{\eta}_d = \mathbf{x}_{d1} = [x_{d11}, x_{d12}, x_{d13}]^T = [x_d, y_d, \psi_d]^T$ .

2) Full-state constraints are satisfied. Under the control input, the state of the surface vessel system does not exceed the predetermined limit. The control objective is mathematically described as  $\lim_{t \rightarrow \infty} \|\mathbf{x}_1(t) - \mathbf{x}_{d1}(t)\| = \vartheta$ , and  $\vartheta \in \mathbb{R}^+$  is an adjustable small constant, where  $\mathbf{x}_1(t) \in \Omega_{x1}$ ,  $\mathbf{x}_2(t) \in \Omega_{x2}$ . The constraint sets are  $\Omega_{x1} := \{x_{1i} \in \mathbb{R}, |x_{1i}| < k_{c1i}, i = 1, 2, 3, t \geq 0\} \subset \mathbb{R}^3$ ,  $\Omega_{x2} := \{x_{2i} \in \mathbb{R}, |x_{2i}| < k_{c2i}, i = 1, 2, 3, t \geq 0\} \subset \mathbb{R}^3$ , where  $k_{c1i}, k_{c2i} \in \mathbb{R}^+$  represent constraint constants.

*Assumption 1:* For any  $k_{c1i} > 0$ , there exist positive vectors  $\mathbf{Y}_1 = [Y_{11}, Y_{12}, Y_{13}]^T$  and  $\mathbf{A}_0 = [A_{00}, A_{01}, A_{02}]^T$ , satisfying  $|x_{d1i}(t)| \leq A_{0(i-1)} < k_{c1i}$ , such that,  $\forall t \geq 0, i = 1, 2, 3$ . The desired trajectory  $\mathbf{x}_{d1}$  and its time derivatives satisfy  $|\dot{x}_{d1i}(t)| \leq Y_{1i}$ .

*Assumption 2:* The external disturbances  $\mathbf{d}(t)$  is bounded, and the Euclidean norm of disturbances vector satisfies  $\|\mathbf{d}(t)\| \leq \bar{d}$ .

*Remark 1:* From the point of view of energy limitation, the external disturbances acting on the surface vessel can be considered as time-varying but bounded signals. Therefore, Assumption 2 is reasonable.

### B. PRELIMINARIES

*Lemma 1 [40]:* For any positive constant  $k_{a1}, k_{b1}$ , let  $Z_1 := \{z_1 \in \mathbb{R} : -k_{a1} < z_1 < k_{b1}\} \subset \mathbb{R}$  and  $N := \mathbb{R}^l \times Z_1 \subset \mathbb{R}^{l+1}$  be open sets. Consider the following system

$$\dot{\eta} = h(t, \eta) \quad (5)$$

where  $\eta := [\omega, z_1]^T \in N$ , and  $h : \mathbb{R}_+ \times N \rightarrow \mathbb{R}^{l+1}$  is piecewise continuous in  $t$  and locally Lipschitz in  $z_1$ , uniformly in  $t$ , on  $\mathbb{R}_+ \times N$ . Suppose that there exist functions  $U : \mathbb{R}^l \rightarrow \mathbb{R}_+$  and  $V_1 : Z_1 \rightarrow \mathbb{R}_+$ , continuously differentiable and definite in their respective domains, such that

$$V_1(z_1) \rightarrow \infty \text{ as } z_1 \rightarrow -k_{a1} \text{ or } z_1 \rightarrow k_{b1} \quad (6)$$

$$\gamma_1(\|\omega\|) \leq U(\omega) \leq \gamma_2(\|\omega\|) \quad (7)$$

where  $\gamma_1$  and  $\gamma_2$  are class  $K_\infty$  functions. Let  $V(\eta) := V_1(z_1) + U(\omega)$ , and  $z_1(0)$  belong to the set  $z_1 \in (-k_{a1}, k_{b1})$ . If the inequality holds:

$$\dot{V} = \frac{\partial V}{\partial \eta} h \leq 0 \quad (8)$$

then  $z_1(t)$  remains in open set  $z_1 \in (-k_{a1}, k_{b1}), \forall t \in [0, \infty)$ .

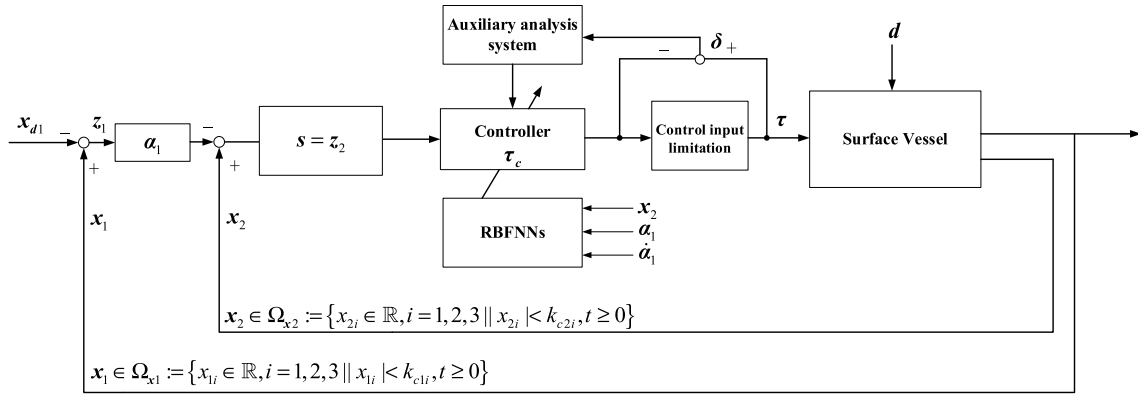


FIGURE 2. The control block diagram of the proposed approach.

Lemma 2 [22]: Considering the dynamic system as follows:

$$\dot{\hat{\phi}}(t) = -r\hat{\phi}(t) + \kappa p(t) \quad (9)$$

where  $r$  and  $\kappa$  are positive constants and  $p(t)$  is a positive definite function. Then, for any given bounded initial condition  $\hat{\phi}(t_0) \geq 0$ , we have  $\hat{\phi}(t) \geq 0$  for  $t \geq t_0$ .

Lemma 3 [16]: The functionals  $V_{x_{1,i}}, i = 1, \dots, n$ , described as  $V_{x_{1,i}}(z_i(t), q_{d_i}(t)) = \int_0^{z_i} [\sigma k_{c_i}^2 d\sigma / k_{c_i}^2 - (\sigma + q_{d_i})^2]$ , satisfy,

$$V_l \leq \frac{k_{cl}^2 z_l^2}{k_{cl}^2 - x_l^2} \quad (10)$$

for  $|x_{1,i}| < k_{c_i}$ .

(2) *RBFNN*: The RBFNN can approximate any nonlinear function in a compact set with arbitrary precision. In control engineering, the RBFNN is typical used to compensate the unknown continuous packaged functions because of its good capabilities in the function approximation [41], [42].

For any unknown continuous function  $f(\mathbf{Z}) : \mathbb{R}^q \rightarrow \mathbb{R}$ , where

$$\mathbf{Z} = [z_1, z_2, \dots, z_q] \in \Omega_{\mathbf{Z}} \quad (11)$$

is the input vector, and  $\Omega_{\mathbf{Z}} \subseteq \mathbb{R}^q$  is a compact set. Thus,

$$f(\mathbf{Z}) = \mathbf{W}^* \mathbf{H}(\mathbf{Z}) + \varepsilon(\mathbf{Z}), \quad \mathbf{Z} \in \Omega_{\mathbf{Z}} \quad (12)$$

in which  $\varepsilon(\mathbf{Z})$  denotes the approximation error, and  $\mathbf{W}^* = [W_1^*, W_2^*, \dots, W_N^*] \in \mathbb{R}^N$  is an optimal weight vector described as

$$\mathbf{W}^* = \arg \min_{\hat{\mathbf{W}} \in \mathbb{R}^q} \left\{ \sup_{\mathbf{Z} \in \Omega_{\mathbf{Z}}} |f(\mathbf{Z}) - \hat{\mathbf{W}}^T \mathbf{H}(\mathbf{Z})| \right\} \quad (13)$$

where  $\hat{\mathbf{W}} \in \mathbb{R}^N$  represents the estimation of  $\mathbf{W}^*$  and  $N$  is the number of neuron nodes in the hidden layer, and  $\mathbf{H}(\mathbf{Z}) = [h_1(\mathbf{Z}), h_2(\mathbf{Z}), \dots, h_N(\mathbf{Z})]^T \in \mathbb{R}^N$  is chosen as the Gaussian basis function vector, which has the following exponential function:

$$h_i(\mathbf{Z}) = \exp \left[ -\frac{\|\mathbf{Z} - \mathbf{c}_i\|^2}{2b_i^2} \right], \quad i = 1, 2, \dots, N \quad (14)$$

where  $\mathbf{c}_i = [c_{i1}, c_{i2}, \dots, c_{iq}]^T$  is the center of the receptive field and  $b_i$  is a positive scalar, and it is the width of the  $j$  th neuron Gaussian function of the hidden layer.

### III. CONTROL DESIGN

In this section, a trajectory tracking control law is presented to achieve the control objective in Section II. The control design process consists of three parts based on the backstepping technique. First, the virtual control law is designed to satisfy output constraints; Second, an actual control law is designed to eliminate the velocity tracking error and satisfied full-state constraints. The neural networks and sliding mode are utilized to process system uncertainties; Third, we set up an auxiliary analysis system to process input saturation. The stability of the closed-loop system is analyzed as well. The overall control block diagram is shown in Fig. 2.

#### A. FULL-STATE CONSTRAINTS

To directly deal with the system state constraints, the iBLF-based control approach is used in system design. The purpose is to make the system state variables  $\mathbf{x}_1(t), \mathbf{x}_2(t)$  satisfies the constraints of  $\mathbf{x}_1(t) \in \Omega_{x1}, \mathbf{x}_2(t) \in \Omega_{x2}$ .

**Step I:** Define the position error vector  $\mathbf{z}_1 = [z_{11}, z_{12}, z_{13}]^T$  as

$$\mathbf{z}_1(t) = \mathbf{x}_1(t) - \mathbf{x}_{d1}(t) \quad (15)$$

Deriving (15) and substituting  $\dot{\mathbf{x}}_1(t)$  into (15) yields

$$\dot{\mathbf{z}}_1(t) = \mathbf{R}(\mathbf{x}_1(t))\mathbf{x}_2(t) - \dot{\mathbf{x}}_{d1}(t) \quad (16)$$

where  $\mathbf{x}_2(t)$  is a virtual control input. The derivative of the component  $\dot{z}_1(t)$  is written as

$$\dot{z}_{1i}(t) = R_i(\mathbf{x}_1(t))x_2(t) - \dot{x}_{d1i}(t) \quad (17)$$

The system state  $\mathbf{x}_1(t)$  need to be constrained. We define the following iBLF as

$$V_{x1}(z_{1i}, x_{d1i}) = \sum_{i=1}^3 \int_0^{z_{1i}} \frac{\Theta_i k_{cl_i}^2}{k_{cl_i}^2 - (\Theta_i + x_{d1i})^2} d\Theta_i \quad (18)$$

where  $\mathbf{x}_1(t) \in \Omega_{\mathbf{x}_1}$ , then  $V_{\mathbf{x}_1}$  is a continuously differentiable and decreasing positive definite function. The following inequality holds.

$$\frac{1}{2} \sum_{i=1}^3 z_{1i}^2 \leq V_{\mathbf{x}_1} \leq \sum_{i=1}^3 z_{1i}^2 \int_0^1 \frac{\omega k_{c1i}^2}{k_{c1i}^2 - (\omega z_{1i} + \text{sgn}(z_{1i})A_{0(i-1)})^2} d\omega \quad (19)$$

The derivative of  $V_{\mathbf{x}_1}$  with respect to time along the subsystem trajectory  $\mathbf{z}_1$  is

$$\begin{aligned} \dot{V}_{\mathbf{x}_1}(t) &= \sum_{i=1}^3 \frac{\partial V_{x1i}}{\partial z_{1i}} \dot{z}_{1i} + \sum_{i=1}^3 \frac{\partial V_{x1i}}{\partial x_{d1i}} \dot{x}_{d1i} \\ &= \sum_{i=1}^3 \frac{k_{c1i}^2 z_{1i} \dot{z}_{1i}}{k_{c1i}^2 - x_{1i}^2} + \sum_{i=1}^3 \frac{\partial V_{x1i}}{\partial x_{d1i}} \dot{x}_{d1i} \end{aligned} \quad (20)$$

Utilizing the approach of integration by parts and the transformation of  $\Theta_i = \omega z_{1i}$ ,  $i = 1, 2, 3$ , we have

$$\sum_{i=1}^3 \frac{\partial V_{x1i}}{\partial x_{d1i}} = \sum_{i=1}^3 z_{1i} \left( \frac{k_{c1i}^2}{k_{c1i}^2 - x_{1i}^2} - \gamma_{1i}(z_{1i}, x_{d1i}) \right) \quad (21)$$

where

$$\gamma_{1i}(z_{1i}, x_{d1i}) = \frac{k_{c1i}}{2z_{1i}} \log \frac{(k_{c1i} + z_{1i} + x_{d1i})(k_{c1i} - x_{d1i})}{(k_{c1i} - z_{1i} - x_{d1i})(k_{c1i} + x_{d1i})}$$

Let  $z_{1i} = 0$ . In terms of the L'Hopital's rule, there exists  $\lim_{t \rightarrow \infty} \gamma_{1i}(z_{1i}, x_{d1i}) = k_{c1i}^2 / (k_{c1i}^2 - x_{d1i}^2)$ . Based on Assumption 1, there is  $\mathbf{x}_1(t) \in \Omega_{\mathbf{x}_1}$ . Therefore,  $\gamma_{1i}(z_{1i}, x_{d1i})$  in the neighborhood of  $z_{1i} = 0$  is defined and bounded.

**Assumption 3:** From Assumption 1, we can furtherly assume that there exists a positive real vector  $\mathbf{A}_1 = [A_{10}, A_{11}, A_{12}]^T$ .  $\alpha_i$  satisfy  $|\alpha_{1i}| \leq A_{1(i-1)} < k_{c2i}$ ,  $i = 1, 2, 3$ .

Design the virtual control law  $\alpha_1(t) = [\alpha_{11}, \alpha_{12}, \alpha_{13}]^T$  as

$$\alpha_1 = \mathbf{R}^T \begin{bmatrix} -\lambda_{11} z_{11} + \frac{k_{c11}^2 - x_{11}^2}{k_{c11}^2} \dot{x}_{d11} \cdot \gamma_{11} \\ -\lambda_{12} z_{12} + \frac{k_{c12}^2 - x_{12}^2}{k_{c12}^2} \dot{x}_{d12} \cdot \gamma_{12} \\ -\lambda_{13} z_{13} + \frac{k_{c13}^2 - x_{13}^2}{k_{c13}^2} \dot{x}_{d13} \cdot \gamma_{13} \end{bmatrix} \quad (22)$$

where  $\lambda_{1i}$ ,  $i = 1, 2, 3$  is positive design parameter.

Based on the above design, we have

$$\dot{V}_{\mathbf{x}_1}(t) = - \sum_{i=1}^3 \frac{\lambda_{1i} k_{c1i}^2 z_{1i}^2}{k_{c1i}^2 - x_{1i}^2} + \sum_{i=1}^3 \frac{k_{c1i}^2 z_{1i} R_i(\mathbf{x}_1) z_{2i}}{k_{c1i}^2 - x_{1i}^2} \quad (23)$$

where  $R_i(\mathbf{x}_1)$  is the  $i$  th line of  $\mathbf{R}(\mathbf{x}_1)$ , and the coupling term  $\sum_{i=1}^3 k_{c1i}^2 z_{1i} R_i(\mathbf{x}_1) z_{2i} / (k_{c1i}^2 - x_{1i}^2)$  will eliminate in the step II.

**Step II:** Define the velocity error vector  $\mathbf{z}_2 = [z_{21}, z_{22}, z_{23}]^T$  as

$$\mathbf{z}_2(t) = \mathbf{x}_2(t) - \alpha_1(t) \quad (24)$$

The system state  $\mathbf{x}_2(t)$  in step II needs to be constrained, therefore, we define the iBLF candidate as

$$V_1 = V_{\mathbf{x}_1}(z_{1i}, x_{d1i}) + V_{\mathbf{x}_2}(z_{2i}, \alpha_{1i}) + \frac{1}{2} \mathbf{z}_2^T \mathbf{M} \mathbf{z}_2 \quad (25)$$

where

$$V_{\mathbf{x}_2} = \sum_{i=1}^3 \int_0^{z_{2i}} \frac{\beta_i k_{c2i}^2}{k_{c2i}^2 - (\beta_i + \alpha_{1i})^2} d\beta_i$$

$V_{\mathbf{x}_2}$  in the set  $\Omega_{\mathbf{x}_2}$  is a continuously differentiable and decreasing positive definite function. The inequality holds

$$\frac{1}{2} \sum_{i=1}^3 z_{2i}^2 \leq V_{\mathbf{x}_2} \leq \sum_{i=1}^3 z_{2i}^2 \int_0^1 \frac{\omega k_{c2i}^2}{k_{c2i}^2 - (\omega z_{2i} + \text{sgn}(z_{2i})A_{1(i-1)})^2} d\omega \quad (26)$$

Under the Assumption 1 and Assumption 3,  $V_1$  in the set  $\Omega_{\mathbf{x}_1}$  and  $\Omega_{\mathbf{x}_2}$  is also a valid candidate for the iBLF. Deriving  $V_1$  with respect to time along the error signal trajectory, we get

$$\begin{aligned} \dot{V}_1(t) &= - \sum_{i=1}^3 \frac{\lambda_{1i} k_{c1i}^2 z_{1i}^2}{k_{c1i}^2 - x_{1i}^2} + \sum_{i=1}^3 \frac{k_{c1i}^2 z_{1i} R_i(\mathbf{x}_1) z_{2i}}{k_{c1i}^2 - x_{1i}^2} \\ &\quad + \sum_{i=1}^3 \frac{k_{c2i}^2 z_{2i} \dot{z}_{2i}}{k_{c2i}^2 - x_{2i}^2} + \sum_{i=1}^3 \frac{\partial V_{x2i}}{\partial \alpha_{1i}} \dot{\alpha}_{1i} + \mathbf{z}_2^T \mathbf{M} \dot{\mathbf{z}}_2 \end{aligned} \quad (27)$$

Utilizing the approach of integration by parts and the transformation of  $\beta_i = \omega z_{2i}$ , we get

$$\sum_{i=1}^3 \frac{\partial V_{x2i}}{\partial \alpha_{1i}} = \sum_{i=1}^3 z_{2i} \left( \frac{k_{c2i}^2}{k_{c2i}^2 - x_{2i}^2} - \gamma_{2i}(z_{2i}, \alpha_{1i}) \right) \quad (28)$$

where

$$\gamma_{2i}(z_{2i}, \alpha_{1i}) = \frac{k_{c2i}}{2z_{2i}} \log \frac{(k_{c2i} + z_{2i} + \alpha_{1i})(k_{c2i} - \alpha_{1i})}{(k_{c2i} - z_{2i} - \alpha_{1i})(k_{c2i} + \alpha_{1i})}$$

Let  $z_{2i} = 0$ . In terms of the L'Hopital's rule, we have  $\lim_{t \rightarrow \infty} \gamma_{2i}(z_{2i}, \alpha_{1i}) = k_{c2i}^2 / (k_{c2i}^2 - \alpha_{1i}^2)$ . Based on Assumption 3, there is  $|\alpha_{1i}| < k_{c2i}$ . Therefore,  $\gamma_{2i}(z_{2i}, \alpha_{1i})$  in the neighborhood  $z_{2i} = 0$  is also defined and bounded.

Differentiating  $\mathbf{z}_2$  with respect to time, we have

$$\dot{\mathbf{z}}_2 = \mathbf{M}^{-1} [\boldsymbol{\tau} + \mathbf{d}(t) - \mathbf{C}(\mathbf{x}_2) \mathbf{x}_2 - \mathbf{D}(\mathbf{x}_2) \mathbf{x}_2] - \dot{\boldsymbol{\alpha}} \quad (29)$$

In terms of the properties of generalized inverses of vectors combining (27) and (29), when  $\mathbf{z}_2 = [0, 0, 0]^T$ ,  $\mathbf{z}_2^T (\mathbf{z}_2^T)^+ = 0$ , we get  $\dot{V}_1 = - \sum_{i=1}^3 (\lambda_{1i} k_{c1i}^2 z_{1i}^2 / (k_{c1i}^2 - x_{1i}^2)) \leq 0$ , which is asymptotically stable by the Barbalat lemma. Considering  $\mathbf{z}_2 \neq [0, 0, 0]^T$ ,  $\mathbf{z}_2^T (\mathbf{z}_2^T)^+ = 1$ , without considering the disturbances, input saturation and the uncertainties of model parameters, the control law is designed as

follows.

$$\begin{aligned} \tau = & -f - Kz_2 - \sum_{i=1}^3 \frac{k_{c1i}^2 z_{1i} R_i^T(x_1)}{k_{c1i}^2 - x_{1i}^2} \\ & - (z_2^T)^+ \sum_{i=1}^3 \left( \frac{k_{c2i}^2 z_{2i} (\dot{z}_{2i} + \dot{\alpha}_{1i})}{k_{c2i}^2 - x_{2i}^2} - z_{2i} \gamma_{2i} \dot{\alpha}_{1i} + \frac{\lambda_{2i} k_{c2i}^2 z_{2i}^2}{k_{c2i}^2 - x_{2i}^2} \right) \end{aligned} \quad (30)$$

where  $f = -C(x_2)x_2 - D(x_2)x_2 - M\dot{\alpha}$  is a continuous function of  $x_1, x_2$  and  $\dot{\alpha}_1, K = K^T \in \mathbb{R}^{3 \times 3}$  is positive definite design matrix,  $R_i^T$  is the  $i$ th line of  $R^T$ , and  $\lambda_{2i} \in \mathbb{R}^+, i = 1, 2, 3$  is positive design parameter.

**B. SYSTEM UNCERTAINTIES**

In practice, the parameters  $M, C(v)$  and  $D(v)$  may be unknown for a surface vessel, and the system is affected by external disturbances  $d(t)$ , which make control law (30) difficult to realize. Due to good approximation performance, RBFNNs are usually used to compensate for unknown continuous function  $f = [f_1, f_2, f_3]^T$  in control law. Then the  $i$ th degree-of-freedom RBFNNs algorithm is

$$h_{ij} = \exp\left(-\frac{\|X_i - c_{ij}\|^2}{2b_{ij}^2}\right), \quad i = 1, 2, \dots, n; j = 1, 2, \dots, m \quad (31)$$

$$f_i = w_i^{*T} h_i + \varepsilon_i \quad (32)$$

where  $X_i$  and basis function  $h_i = [h_{i1}, h_{i2}, \dots, h_{im}]^T$  are the input and output of the  $i$ th network, respectively;  $\varepsilon_i$  and  $w_i^*$  are the  $i$ th neural network approximation error and ideal weight, respectively.

Yin *et al.* [20] used the RBFNNs to approximate the uncertainties in the system. and the adaptive control of neural network without model information is realized. The unknown nonlinear function  $f \in \mathbb{R}^3$  in each degree-of-freedom needs to be approximated by neural network and estimated by adaptive parameters. However, too many parameters need to be adjusted, which will increase the difficulty and complexity of system performance adjustment and analysis, and also bring inconvenience to real-time control.

To solve above problem, a single parameter online adjustment is introduced to replace the weights of the neural network to realize adaptive control based on single parameter. Therefore, we take  $\hat{w}_i$  as the estimation weight vector of  $i$ th neural networks. Let  $\tilde{w}_i = w_i^* - \hat{w}_i$ , The Frobenius norm of  $w_i^*$  satisfies  $\|w_i^*\|_F \leq w_{imax}$ , and we define a single parameter as

$$\xi = \max \left\{ \|w_i^*\|^2, i = 1, 2, 3 \right\} \quad (33)$$

where  $\xi \in \mathbb{R}^+$ , obviously  $\xi$  is an unknown positive constant because  $\|w_i^*\|$  is unknown. Define  $\hat{\xi}$  as an estimate value of  $\xi, \hat{W} = [\hat{w}_1^T, \hat{w}_2^T, \hat{w}_3^T]$  as an estimate weigh matrix of  $W^* = [w_1^{*T}, w_2^{*T}, w_3^{*T}]$ , then we get  $\tilde{\xi} = \hat{\xi} - \xi, \tilde{W} = W^* - \hat{W}$ . Define  $h(X) = [h_1^T, h_2^T, h_3^T]^T$  as basis

function,  $X = [x_2^T, \alpha_1^T, \dot{\alpha}_1^T]^T$  is the input vector to the neural network. We can utilize the following operators [44].

$$\begin{aligned} W^* \circ h(X) &= [w_1^{*T} h_1, w_2^{*T} h_2, w_3^{*T} h_3]^T \\ \hat{W} \circ h(X) &= [\hat{w}_1^T h_1, \hat{w}_2^T h_2, \hat{w}_3^T h_3]^T \\ h(X) \circ h(X) &= [h_1^T h_1, h_2^T h_2, h_3^T h_3]^T \\ z_2 \circ z_2 &= [z_{21}^T z_{21}, z_{22}^T z_{22}, z_{23}^T z_{23}]^T \end{aligned} \quad (34)$$

The neural networks  $\hat{W} \circ h(X)$  approximates  $W^* \circ h(X)$ , that is  $\hat{f} = \hat{W} \circ h$  approximates  $f = W^* \circ h + \varepsilon, \varepsilon = [\varepsilon_1, \varepsilon_2, \varepsilon_3]^T$ . then we have  $\tilde{f} = f - \hat{f}$ .

*Assumption 4:* For all  $X \in \Omega_X$ , the approximation error  $\varepsilon(X)$  is bounded by a positive constant  $\varepsilon_N$ . That is  $\|\varepsilon\| \leq \varepsilon_N$ .

We define the following functions as:

$$H(z_2) = \begin{cases} 0, & z_2 = [0, 0, 0]^T \\ 1, & \text{Otherwise} \end{cases} \quad (35)$$

Consider  $z_2 = [0, 0, 0]^T$  from a practical point of view, once the system reaches the origin, control performance is the best, that is not necessary to take control action for less power consumption [43]. From (23) to (28), we can easily get  $\dot{V}_1 \leq 0$  without considering the neural networks. The Barbalat lemma can be employed to prove the stability in this case.

If the neural network approximates the unknown nonlinear function to compensate for the control law, we need to consider the Lyapunov function candidate as  $V = V_1 + \tilde{\xi}^2 / 2r$ . Here, the single parameter error energy function  $\xi$  is introduced to replace the weights estimation matrix of the neural networks in the closed-loop system.

For the unknown parameter  $\xi$ , the adaptive law is designed as follows.

$$\dot{\hat{\xi}} = H(z_2) \left[ \frac{r}{2a^2} \sum_{i=1}^3 z_{2i}^2 \|h_i\|^2 - \varpi r \hat{\xi} \right] \quad (36)$$

where  $r > 0, a > 0, \varpi > 0$ .  $\varpi r$  indicates that the correction constant is used to prevent the estimate value from increasing to the maximum, so as to enhance the robustness of the closed-loop system.

*Remark 2:* From Lemma 2, when  $\hat{\xi}(0) \geq 0$ , then for all  $t \geq 0$ , we have  $\hat{\xi}(t) \geq 0$ . In fact, utilizing  $\hat{\xi}$  as an estimate of  $\xi$  for  $\hat{\xi}(0) \geq 0$  is always reasonable in the actual situations.

The advantage of sliding mode control is used to overcome the approximation error. Considering the backstepping control design step II, the sliding mode variable structure control is introduced as follows.

$$s = z_2 \quad (37)$$

Derivation of equation (37) combined with (27), (29), (33) and (36), the control law yields,

$$\begin{aligned} \tau = H(z_2) \left\{ - \sum_{i=1}^3 \frac{k_{c1i}^2 z_{1i} R_i^T(x_1)}{k_{c1i}^2 - x_{1i}^2} - Kz_2 - \frac{1}{2a^2} z_2 \hat{\xi} \circ (h \circ h) \right. \\ \left. - (z_2^T)^+ (\cdot) - \bar{\eta} \text{sgn}(z_2) \right\} \end{aligned} \quad (38)$$

where  $(\cdot)$  is the right term of the generalized inverse  $(z_2^T)^+$  in equation (30), and  $-\bar{\eta}\text{sgn}(z_2)$  is a robust term to overcome the neural network approximation error  $\mathbf{e}$ , where  $\bar{\eta} = \varepsilon_N + \bar{d}$ ,  $\text{sgn}(z_2) = \text{diag}(\text{sgn}(z_{21}), \text{sgn}(z_{22}), \text{sgn}(z_{23}))$ .

*Remark 3:* It is worth noting that  $z_2 = [0, 0, 0]^T$  implies the perfect tracking performance of the systems output and the control action should not be taken and the adaptive law  $\dot{\xi} = 0$ . For  $z_2 \neq [0, 0, 0]^T$ , the controller takes control action, and the adaptive law begins to update online.

**C. INPUT SATURATION**

The input saturation is that system actuator can only provide a limited range of control signals. Due to the physical limitations of the vessel actuators, large control forces and moments are difficult to achieve. Here, input saturation compensation can be achieved by defining a auxiliary analysis system. The auxiliary analysis system is defined as follows:

$$\dot{\mathbf{e}} = H(z_2) \begin{cases} -\mathbf{K}_e \mathbf{e} - \frac{1}{\|\mathbf{e}\|^2} f(z_{2i}, \delta_i) \mathbf{e} + \boldsymbol{\delta}, & \|\mathbf{e}\| \geq \sigma \\ [0, 0, 0]^T, & \|\mathbf{e}\| < \sigma \end{cases} \quad (39)$$

where  $f(z_{2i}, \delta_i) = \sum_{i=1}^3 |z_{2i} \delta_i| + 0.5 \boldsymbol{\delta}^T \boldsymbol{\delta}$ ,  $\mathbf{e} = [e_1, e_2, e_3]^T$  is the state vector of the auxiliary analysis system,  $\mathbf{K}_e = \mathbf{K}_e^T \in \mathbb{R}^{3 \times 3}$  is a positive definite design matrix,  $\boldsymbol{\delta} = \boldsymbol{\tau} - \boldsymbol{\tau}_c$ , and  $\sigma > 0$  is a small design constant. The auxiliary analysis system (39) can avoid the singularity problem due to taking  $\dot{\mathbf{e}} = [0, 0, 0]^T$  when  $\|\mathbf{e}\| < \sigma$ .

*Remark 4:* The input saturation needs to satisfy the actual physical conditions. That is, there is always a control input, which enables the system to achieve output tracking with input saturation.

Finally, we design the control law as follows.

$$\boldsymbol{\tau}_c = H(z_2) \left\{ - \sum_{i=1}^3 \frac{k_{c1i}^2 z_{1i} R_i^T(\mathbf{x}_1)}{k_{c1i}^2 - x_{1i}^2} - \mathbf{K} z_2 - \frac{1}{2a^2} z_2 \hat{\xi} \circ (\mathbf{h} \circ \mathbf{h}) + \mathbf{K}_h \mathbf{e} - (z_2^T)^+ (\cdot) - \bar{\eta} \text{sgn}(z_2) \right\} \quad (40)$$

where  $\mathbf{K}_h = \mathbf{K}_h^T \in \mathbb{R}^{3 \times 3}$  is positive definite designed matrix.

According to the above three parts, we can conclude the following theorem.

*Theorem 1:* Consider the surface vessel (1) in the presence of full-state constraints, input saturation, and unknown uncertainties under Assumptions 1-4. If the initial conditions satisfies  $\mathbf{x}_1(0) \in \Omega_{x1} := \{x_{1i} \in \mathbb{R}, |x_{1i}| < k_{c1i}, i = 1, 2, 3\}$   $\mathbf{x}_2(0) \in \Omega_{x2} := \{x_{2i} \in \mathbb{R}, |x_{2i}| < k_{c2i}, i = 1, 2, 3\}$ , under the virtual control law (22), actual control law (40), and adaptation law (36), then the following conclusions hold.

- 1) The tracking errors are bounded.
- 2) The system full-state constraints are never violated.
- 3) All signals in closed-loop system are bounded.

The stability of the closed-loop control system are respectively discussed as follows.

*Proof:*

**A).** When  $z_2 \neq [0, 0, 0]^T$ .

1). Select the Lyapunov function candidate for the whole closed-loop system consisting of (1), (33), (37), (39) as

$$V_2 = V_{x1}(z_{1i}, x_{d1i}) + V_{x2}(z_{2i}, \alpha_{1i}) + \frac{1}{2} z_2^T \mathbf{M} z_2 + \frac{1}{2r} \tilde{\xi}^2 + \frac{1}{2} \mathbf{e}^T \mathbf{e} \quad (41)$$

Differentiating the equation in (41) with respect to time, and substituting equations (27), (29), (35), (36), (37), (39) and  $\boldsymbol{\tau} = \boldsymbol{\tau}_c + \boldsymbol{\delta}$  into  $\dot{V}_2$  yields

$$\begin{aligned} \dot{V}_2(t) = & - \sum_{i=1}^3 \frac{\lambda_{1i} k_{c1i}^2 z_{1i}^2}{k_{c1i}^2 - x_{1i}^2} - \sum_{i=1}^3 \frac{\lambda_{2i} k_{c2i}^2 z_{2i}^2}{k_{c2i}^2 - x_{2i}^2} \\ & + z_2^T \left[ -\frac{1}{2a^2} z_2 \hat{\xi} \circ (\mathbf{h} \circ \mathbf{h}) + \mathbf{W}^* \circ \mathbf{h} \right] \\ & - z_2^T \mathbf{K} z_2 + z_2^T [\mathbf{e} + \mathbf{d} - \bar{\eta} \text{sgn}(z_2)] + z_2^T \mathbf{K}_h \mathbf{e} \\ & + z_2^T \boldsymbol{\delta} + \mathbf{e}^T \dot{\mathbf{e}} + \frac{1}{2a^2} \tilde{\xi} \sum_{i=1}^3 z_{2i}^2 \|\mathbf{h}_i\|^2 - \varpi \tilde{\xi} \hat{\xi} \end{aligned} \quad (42)$$

For the auxiliary analysis system, we consider the following two sides.

(a) When  $\|\mathbf{e}\| \geq \sigma$ , in terms of (39) and Young's inequality, we obtain

$$\begin{aligned} \mathbf{e}^T \dot{\mathbf{e}} = & -\mathbf{e}^T \mathbf{K}_e \mathbf{e} - \sum_{i=1}^3 |z_{2i} \delta_i| - \frac{1}{2} \boldsymbol{\delta}^T \boldsymbol{\delta} + \mathbf{e}^T \boldsymbol{\delta} \\ \leq & -\mathbf{e}^T \mathbf{K}_e \mathbf{e} - \sum_{i=1}^3 |z_{2i} \delta_i| + \frac{1}{2} \mathbf{e}^T \mathbf{e} \end{aligned} \quad (43)$$

Expanding terms  $z_2^T [\mathbf{W}^* \circ \mathbf{h}]$  and  $z_2^T [-z_2 \hat{\xi} \circ (\mathbf{h} \circ \mathbf{h})/2a^2]$  in equation (42), we obtain

$$\begin{aligned} z_2^T [\mathbf{W}^* \circ \mathbf{h}] = & [z_{21}, z_{22}, z_{23}] \begin{bmatrix} \mathbf{w}_1^{*T} \mathbf{h}_1 \\ \mathbf{w}_2^{*T} \mathbf{h}_2 \\ \mathbf{w}_3^{*T} \mathbf{h}_3 \end{bmatrix} \\ = & \sum_{i=1}^3 z_{2i} \mathbf{w}_i^{*T} \mathbf{h}_i \\ z_2^T \left[ -\frac{1}{2a^2} z_2 \hat{\xi} \circ (\mathbf{h} \circ \mathbf{h}) \right] = & -\frac{1}{2a^2} \hat{\xi} [z_{21}, z_{22}, z_{23}] \\ & \times \left( \begin{bmatrix} z_{21} \\ z_{22} \\ z_{23} \end{bmatrix} \circ \begin{bmatrix} \mathbf{h}_1^T \mathbf{h}_1 \\ \mathbf{h}_2^T \mathbf{h}_2 \\ \mathbf{h}_3^T \mathbf{h}_3 \end{bmatrix} \right) \\ = & -\frac{1}{2a^2} \hat{\xi} \sum_{i=1}^3 z_{2i}^2 \|\mathbf{h}_i\|^2 \end{aligned} \quad (44)$$

In the light of equation (44) and Young's inequality, taking the maximum value  $\xi$  of  $\|\mathbf{w}_i^*\|^2$ , we obtain

$$z_2^T [\mathbf{W}^* \circ \mathbf{h}] \leq \frac{1}{2a^2} \xi \sum_{i=1}^3 z_{2i}^2 \mathbf{h}_i^T \mathbf{h}_i + \frac{3}{2} a^2 \quad (46)$$

Continuing to utilize Young's inequality, we obtain

$$-\varpi \tilde{\xi} \hat{\xi} \leq -\frac{\varpi}{2} \tilde{\xi}^2 + \frac{\varpi}{2} \xi^2 \quad (47)$$

Substituting (43), (45), (46) and (47) into (42), we obtain

$$\begin{aligned} \dot{V}_2(t) &\leq -\sum_{i=1}^3 \frac{\lambda_{1i} k_{c1i}^2 z_{1i}^2}{k_{c1i}^2 - x_{1i}^2} - \sum_{i=1}^3 \frac{\lambda_{2i} k_{c2i}^2 z_{2i}^2}{k_{c2i}^2 - x_{2i}^2} - z_2^T \mathbf{K} z_2 \\ &\quad + \frac{1}{2} z_2^T z_2 + \frac{1}{2} e^T \mathbf{K}_h^T \mathbf{K}_h e + z_2^T \delta - e^T \mathbf{K}_e e \\ &\quad - \sum_{i=1}^3 |z_{2i} \delta_i| + \frac{1}{2} e^T e - \frac{\varpi}{2} \tilde{\xi}^2 + \frac{\varpi}{2} \xi + \frac{3}{2} a^2 \\ &\leq -\sum_{i=1}^3 \frac{\lambda_{1i} k_{c1i}^2 z_{1i}^2}{k_{c1i}^2 - x_{1i}^2} - \sum_{i=1}^3 \frac{\lambda_{2i} k_{c2i}^2 z_{2i}^2}{k_{c2i}^2 - x_{2i}^2} \\ &\quad - \left[ \lambda_{\min}(\mathbf{K}) - \frac{1}{2} \right] z_2^T z_2 \\ &\quad - \left[ \lambda_{\min} \left( \mathbf{K}_e - \frac{1}{2} \mathbf{K}_h^T \mathbf{K}_h \right) - \frac{1}{2} \right] e^T e - \frac{\varpi}{2} \tilde{\xi}^2 \\ &\quad + \frac{\varpi}{2} \xi^2 + \frac{3}{2} a^2 \end{aligned} \quad (48)$$

Based on Lemma 3, the following inequalities are easy to be proven that

$$-\sum_{i=1}^3 \frac{\lambda_{1i} k_{c1i}^2 z_{1i}^2}{k_{c1i}^2 - x_{1i}^2} \leq -\sum_{i=1}^3 \int_0^{z_{1i}} \frac{\lambda_{1i} k_{c1i}^2 \Theta_i}{k_{c1i}^2 - (\Theta_i + x_{d1i})^2} d\Theta_i \quad (49)$$

$$-\sum_{i=1}^3 \frac{\lambda_{2i} k_{c2i}^2 z_{2i}^2}{k_{c2i}^2 - x_{2i}^2} \leq -\sum_{i=1}^3 \int_0^{z_{2i}} \frac{\lambda_{2i} k_{c2i}^2 \beta_i}{k_{c2i}^2 - (\beta_i + \alpha_{1i})^2} d\beta_i \quad (50)$$

then

$$\dot{V}_2(t) \leq -\rho_1 V_2(t) + C_1 \quad (51)$$

where  $\rho_1$  with  $C_1$  are positive constants.

$$\rho_1 = \min \left\{ \min(\lambda_{1i}), \min(\lambda_{2i}), \frac{2 \left[ \lambda_{\min}(\mathbf{K}) - \frac{1}{2} \right]}{\lambda_{\max}(\mathbf{M})}, \right. \\ \left. 2 \left[ \lambda_{\min} \left( \mathbf{K}_e - \frac{1}{2} \mathbf{K}_h^T \mathbf{K}_h \right) - \frac{1}{2} \right], \varpi r \right\} \quad (52)$$

$$C_1 = \frac{\varpi}{2} \xi^2 + \frac{3}{2} a^2 \quad (53)$$

where  $\lambda_{\min}(\cdot)$  and  $\lambda_{\max}(\cdot)$  are defined as the minimum and the maximum eigenvalues of the matrix  $(\cdot)$ , respectively.

(b) When  $\|e\| < \sigma$ , in terms of (39) and Young's inequality, obtain

$$e^T \dot{e} = 0 \quad (54)$$

$$\frac{1}{2} e^T \mathbf{K}_h^T \mathbf{K}_h e < -\frac{1}{2} e^T \mathbf{K}_h^T \mathbf{K}_h e + \sigma^2 \|\mathbf{K}_h^T \mathbf{K}_h\| \quad (55)$$

$$z_2^T \delta \leq \frac{1}{2} z_2^T z_2 + \frac{1}{2} \|\delta\|^2 \quad (56)$$

Substituting (43), (45), (46) and (47) into (42), and utilizing (54)-(56), we obtain

$$\begin{aligned} \dot{V}_2(t) &= -\sum_{i=1}^3 \frac{\lambda_{1i} k_{c1i}^2 z_{1i}^2}{k_{c1i}^2 - x_{1i}^2} - \sum_{i=1}^3 \frac{\lambda_{2i} k_{c2i}^2 z_{2i}^2}{k_{c2i}^2 - x_{2i}^2} \\ &\quad + z_2^T \left[ -\frac{1}{2a^2} z_2 \hat{\xi} \circ (\mathbf{h} \circ \mathbf{h}) + \mathbf{W}^* \circ \mathbf{h} \right] \\ &\quad - z_2^T \mathbf{K} z_2 + z_2^T [\mathbf{e} + \mathbf{d} - \bar{\eta} \text{sgn}(z_2)] + z_2^T \mathbf{K}_h e \end{aligned}$$

$$\begin{aligned} &+ z_2^T \delta + \frac{1}{2a^2} \tilde{\xi} \sum_{i=1}^3 z_{2i}^2 \|\mathbf{h}_i\|^2 - \varpi \tilde{\xi} \hat{\xi} \\ &\leq -\sum_{i=1}^3 \frac{\lambda_{1i} k_{c1i}^2 z_{1i}^2}{k_{c1i}^2 - x_{1i}^2} - \sum_{i=1}^3 \frac{\lambda_{2i} k_{c2i}^2 z_{2i}^2}{k_{c2i}^2 - x_{2i}^2} - z_2^T \mathbf{K} z_2 + z_2^T z_2 \\ &\quad - \frac{1}{2} e^T \mathbf{K}_h^T \mathbf{K}_h e + \sigma^2 \|\mathbf{K}_h^T \mathbf{K}_h\| + \frac{1}{2} \|\delta\|^2 - \frac{\varpi}{2} \tilde{\xi}^2 \\ &\quad + \frac{\varpi}{2} \xi^2 + \frac{3}{2} a^2 \\ &\leq -\sum_{i=1}^3 \frac{\lambda_{1i} k_{c1i}^2 z_{1i}^2}{k_{c1i}^2 - x_{1i}^2} - \sum_{i=1}^3 \frac{\lambda_{2i} k_{c2i}^2 z_{2i}^2}{k_{c2i}^2 - x_{2i}^2} \\ &\quad - [\lambda_{\min}(\mathbf{K}) - 1] z_2^T z_2 \\ &\quad - \frac{1}{2} \lambda_{\min}(\mathbf{K}_h^T \mathbf{K}_h) e^T e - \frac{\varpi}{2} \tilde{\xi}^2 + \sigma^2 \|\mathbf{K}_h^T \mathbf{K}_h\| \\ &\quad + \frac{1}{2} \|\delta\|^2 + \frac{\varpi}{2} \xi^2 + \frac{3}{2} a^2 \end{aligned} \quad (57)$$

Similarly, we use (49) and (50) to get

$$\dot{V}_2(t) \leq -\rho_2 V_2(t) + C_2 \quad (58)$$

where  $\rho_2$  and  $C_2$  are positive constants

$$\rho_2 = \min \left\{ \min(\lambda_{1i}), \min(\lambda_{2i}), \frac{2 [\lambda_{\min}(\mathbf{K}) - 1]}{\lambda_{\max}(\mathbf{M})}, \right. \\ \left. \lambda_{\min}(\mathbf{K}_h^T \mathbf{K}_h), \frac{\varpi r}{\varpi r} \right\} \quad (59)$$

$$C_2 = \sigma^2 \|\mathbf{K}_h^T \mathbf{K}_h\|^2 + \frac{1}{2} \|\delta\|^2 + \frac{\varpi}{2} \xi^2 + \frac{3}{2} a^2 \quad (60)$$

Synthesizing (51) and (58), we obtain

$$\dot{V}_2(t) \leq -\rho V_2(t) + C \quad (61)$$

where  $\rho = \min(\rho_1, \rho_2)$ ,  $C = \max(C_1, C_2)$ . To ensure  $\rho > 0$ , the design parameters  $\mathbf{K}$ ,  $\mathbf{K}_h$ , and  $\mathbf{K}_e$  satisfy the following conditions:

$$\lambda_{\min}(\mathbf{K}) > 1 \quad (62)$$

$$\lambda_{\min} \left( \mathbf{K}_e - \frac{1}{2} \mathbf{K}_h^T \mathbf{K}_h \right) > \frac{1}{2} \quad (63)$$

Multiplying both sides of inequality (61) by  $e^{\rho t}$ , we obtain

$$\frac{d}{dt} (V_2(t) e^{\rho t}) \leq C e^{\rho t} \quad (64)$$

Integrating (64) over  $[0, t]$ , (64) further becomes

$$0 \leq V_2(t) \leq \frac{C}{\rho} + \left( V_2(0) - \frac{C}{\rho} \right) e^{-\rho t} \leq V_2(0) e^{-\rho t} + \frac{C}{\rho} \quad (65)$$

It's well known that every term in (41) is positive, then the following inequality holds:

$$\begin{aligned} \frac{1}{2} \sum_{i=1}^3 z_{1i}^2 &\leq \sum_{i=1}^3 \int_0^{z_{1i}} \frac{\Theta_i k_{c1i}^2}{k_{c1i}^2 - (\Theta_i + x_{d1i})^2} d\Theta_i \\ &\leq V_2(t) \leq V_2(0) e^{-\rho t} + \frac{C}{\rho} \end{aligned} \quad (66)$$

$$\frac{1}{2} \sum_{i=1}^3 z_{2i}^2 \leq \sum_{i=1}^3 \int_0^{z_{2i}} \frac{\beta_i k_{c2i}^2}{k_{c2i}^2 - (\beta_i + \alpha_{1i})^2} d\beta_i \leq V_2(t) \leq V_2(0)e^{-\rho t} + \frac{C}{\rho} \quad (67)$$

$$\frac{1}{2} z_2^T M z_2 \leq V_2(t) \leq V_2(0)e^{-\rho t} + \frac{C}{\rho} \quad (68)$$

From equation (41), we can obtain

$$V_2(0) = \sum_{i=1}^3 \int_0^{z_{1i}(0)} \frac{\Theta_i k_{c1i}^2}{k_{c1i}^2 - (\Theta_i + x_{d1i}(0))^2} d\Theta_i + \sum_{i=1}^3 \int_0^{z_{2i}(0)} \frac{\beta_i k_{c2i}^2}{k_{c2i}^2 - (\beta_i + \alpha_{1i}(0))^2} d\beta_i + \frac{1}{2} \|z_2(0)\|^2 + \frac{1}{2r} |\hat{\xi}(0) - \xi|^2 + \frac{1}{2} \|e(0)\|^2 \quad (69)$$

Then, the compact set of the error signals  $z_1$  and  $z_2$  are obtained as

$$\Omega_{z_1} := \left\{ z_1(t) \in \mathbb{R}^3 \mid \|z_1(t)\| \leq \sqrt{W}, t \geq 0 \right\}$$

$$\Omega_{z_2} := \left\{ z_2(t) \in \mathbb{R}^3 \mid \|z_2(t)\| \leq \sqrt{W}, t \geq 0 \right\}$$

$$\cap \left\{ z_2(t) \in \mathbb{R}^3 \mid \|z_2(t)\| \leq \sqrt{\frac{W}{\lambda_{\max}(M)}}, t \geq 0 \right\}$$

Similarly, we have

$$\frac{1}{2} \tilde{\xi}^2 \leq V_2(t) \leq V_2(0)e^{-\rho t} + \frac{C}{\rho} \quad (70)$$

The compact set of the error signals  $\tilde{\xi}$  is obtained

$$\Omega_{\tilde{\xi}} := \left\{ \tilde{\xi}(t) \in \mathbb{R} \mid |\tilde{\xi}(t)| \leq \sqrt{Wr}, t \geq 0 \right\}$$

where  $W = 2(V_2(0) + C/\rho)$ .

(2) In terms of (65), let  $V_2(0) + C/\rho \triangleq b \in \mathbb{R}^+$ , and we have  $V_2(t) \leq b, \forall t \geq 0$ . According to the definition of the BLF, it can conclude  $V_2(t) \rightarrow \infty$ . When  $|x_{1i}| \rightarrow \infty$  and  $|x_{2i}| \rightarrow \infty, i = 1, 2, 3$ . Because of the boundedness of  $V_2(t)$ , we know that  $|x_{1i}| \neq k_{c1i}$  and  $|x_{2i}| \neq k_{c2i}$ , which always remain in the constraint sets  $\Omega_{x_1}$  and  $\Omega_{x_2}$ . Similarly, based on Lemma 1,  $x_1(t)$  and  $x_2(t)$  are kept in their respective constraint sets  $\Omega_{x_1}$  and  $\Omega_{x_2}$  under the initial conditions  $x_1(0) \in \Omega_{x_1}$  and  $x_2(0) \in \Omega_{x_2}, \forall t \geq 0$ .

(3) By choosing the appropriate parameter  $\lambda_{1i}$  to satisfy the initial condition  $|\alpha_{1i}(0)| < k_{c2i}, |\alpha_{1i}(t)| < k_{c2i}$  can be obtained under the control law. It has been proved in 2) that there is  $|x_{2i}| < k_{c2i}$ , where  $|x_{2i}| = |z_{2i} + \alpha_{1i}|$ , so we get  $|\alpha_{1i}(t)| < k_{c2i}, i = 1, 2, 3, \forall t \geq 0$  under Assumption 3. From (36), it can be in turn verified the boundedness of adaptive laws  $\hat{\xi}$ . From (65) we can conclude that auxiliary design variable  $e$  is bounded, and converge to a compact set asymptotically. The proof of Theorem 1 above shows that input saturation exists when the auxiliary design system satisfy the condition  $\|e\| \geq \sigma$ . If  $\|e\| < \sigma$ , it means that there is no input saturation, then we get  $\delta = [0, 0, 0]^T$ , so  $\tau = \tau_c$

and the control input  $\tau$  is bounded. Thus,  $\tau_c$  is bounded. Consequently, all signals in closed-loop system are bounded.

*Remark 5:* The constraint constants  $k_{c1i}$  and  $k_{c2i}$  considered here can be given according to the actual operation requirements of the system. Furthermore, the state constraint constants need to satisfy condition  $k_{c1i} > |x_{d1i}|, k_{c2i} > |\alpha_{1i}|, i = 1, 2, 3$ .

**B).** Once  $z_2 = [0, 0, 0]^T$ , which means the control effect has reached the best, the control action will not be taken.

Based on (36), (39) and (40), it is easy to know that the adaptive law  $\dot{\hat{\xi}} = 0$ , the auxiliary design variable  $e = [0, 0, 0]^T$  and the control law  $\tau_c = [0, 0, 0]^T$ , such that the Lyapunov functions  $V_2$  in (41) can be rewritten as

$$V_2 = \sum_{i=1}^3 \int_0^{z_{1i}} \frac{\Theta_i k_{c1i}^2}{k_{c1i}^2 - (\Theta_i + x_{d1i})^2} d\Theta_i \quad (71)$$

Differentiating the equation (71) with respect to time, then substituting (17) and (21) yields

$$\dot{V}_2 = - \sum_{i=1}^3 \frac{\lambda_{1i} k_{c1i}^2 z_{1i}^2}{k_{c1i}^2 - x_{1i}^2} + \sum_{i=1}^3 \frac{k_{c1i}^2 z_{1i} R_i(x_1) z_2}{k_{c1i}^2 - x_{1i}^2} \quad (72)$$

Substituting  $z_2 = [0, 0, 0]^T$  into (72), we obtain

$$\dot{V}_2 = - \sum_{i=1}^3 \frac{\lambda_{1i} k_{c1i}^2 z_{1i}^2}{k_{c1i}^2 - x_{1i}^2} \leq 0 \quad (73)$$

It's easy to get  $V_2(t) \leq V_2(0), \forall t \geq 0$  from the property of  $V_2$ . Based on (71), we obtain

$$\frac{1}{2} \sum_{i=1}^3 z_{1i}^2 \leq V_2(t) = \sum_{i=1}^3 \int_0^{z_{1i}} \frac{\Theta_i k_{c1i}^2}{k_{c1i}^2 - (\Theta_i + x_{d1i})^2} d\Theta_i \leq V_2(0) \quad (74)$$

where  $V_2(0) = \sum_{i=1}^3 \int_0^{z_{1i}(0)} \Theta_i k_{c1i}^2 d\Theta_i / k_{c1i}^2 - (\Theta_i + x_{d1i}(0))^2$ .

The compact set of the error  $z_1$  is obtained as

$$\Omega_{z_1} := \left\{ z_1(t) \in \mathbb{R}^3 \mid \|z_1(t)\| \leq \sqrt{2V_2(0)}, t \geq 0 \right\}$$

Similarly, it is easy to prove that the closed-loop system signals are bounded and the state does not violate the constraints according to the discussion in **A**).

The proof is ended for the discussions about two institutions.

#### IV. SIMULATIONS

In this section, to validate the proposed control approach, a simulation is carry out on the tested vessel CyberShip II [45], [46]. We divide the simulation into two parts. Part I: the desired position trajectory is an ellipse. Part II: The desired position trajectory is similar to [19], it is a more general trajectory.

The desired position trajectories of Part I and Part II are chosen as follows

Let  $\mathbf{x}_{d1} = [x_{d11}, x_{d12}, x_{d13}]^T = \boldsymbol{\eta}_d = [x_d, y_d, \psi_d]^T$ , where Part I:  $x_d = 100 \cos t, y_d = 50 \sin t, \psi_d = \tan^{-1} \frac{\dot{y}_d}{\dot{x}_d}$ , Part II:  $x_d = 5 \sin 0.5t, y_d = 10 \cos 1.1t, \psi_d = \frac{\pi}{2} \sin t$ .

The system model parameters are given as below.

The inertia matrix  $\mathbf{M}$

$$\mathbf{M} = \begin{bmatrix} m_{11} & 0 & 0 \\ 0 & m_{22} & m_{23} \\ 0 & m_{32} & m_{33} \end{bmatrix}$$

$$m_{11} = m - X_{\dot{u}}$$

$$m_{22} = m - Y_{\dot{v}}$$

$$m_{23} = m - Y_{\dot{v}}$$

$$m_{32} = m x_g - N_{\dot{v}}$$

$$m_{33} = I_z - N_{\dot{r}}$$

The centripetal and Coriolis torques matrix  $\mathbf{C}(\mathbf{v})$

$$\mathbf{C}(\mathbf{v}) = \begin{bmatrix} 0 & 0 & c_{13} \\ 0 & 0 & c_{23} \\ c_{31} & c_{32} & 0 \end{bmatrix}$$

$$c_{13} = -(m - Y_{\dot{v}})v - (m x_g - Y_{\dot{r}})r$$

$$c_{23} = (m - X_{\dot{u}})u$$

$$c_{31} = (m - Y_{\dot{v}})v + m x_g$$

$$c_{32} = -(m - X_{\dot{u}})u$$

and the hydrodynamic damping matrix  $\mathbf{D}(\mathbf{v})$

$$\mathbf{D}(\mathbf{v}) = \begin{bmatrix} d_{11} & 0 & 0 \\ 0 & d_{22} & d_{23} \\ 0 & d_{32} & d_{33} \end{bmatrix}$$

$$d_{11} = -X_u - X_{uu}|u| - X_{uuu}u^2$$

$$d_{22} = -Y_v - Y_{vv}|v| - Y_{rv}|r|$$

$$d_{23} = -Y_r - Y_{vr}|v| - Y_{rr}|r|$$

$$d_{32} = -N_v - N_{vv}|v| - N_{rv}|r|$$

$$d_{33} = -N_r - N_{vr}|v| - N_{rr}|r|$$

where  $m = 23.8, x_g = 0.046, X_{\dot{u}} = -2, Y_{\dot{v}} = -10, Y_{\dot{r}} = 0, N_{\dot{v}} = 0, N_{\dot{r}} = -1, X_u = -0.7225, X_{uu} = -1.3274, X_{uuu} = -5.8664, Y_v = -0.8612, Y_{vv} = -36.2832, Y_{rv} = 0, Y_r = 0.1079, Y_{vr} = 0, Y_{rr} = 0, N_v = 0.1052, N_{vv} = 5.0437, N_{rv} = 0, N_r = -0.5, N_{vr} = 0, N_{rr} = 0$ .

**Part I:** The initial values of the surface vessel are chosen as  $\boldsymbol{\eta}(0) = [101, -1, 0]^T$  and  $\mathbf{v}(0) = [5, -0.5, -0.3]^T$ . The constraints are  $\mathbf{k}_{c1} = [102, 51, 3.3]^T$  and  $\mathbf{k}_{c2} = [10.2, 6, 0.8]^T$ , respectively. The disturbance vector is chosen as  $\mathbf{d}(t) = [0.25 \sin(t), 0.25 \sin(t), 0.25 \sin(t)]^T$ . The width of the neuron Gaussian function of the hidden layer  $b_{ij}$  are all 50. The center  $\mathbf{c}_{ij}$  in (31) are all  $9 \times 512$  matrices, whose elements are 1 and -1. The updated parameters in (36) are  $\varpi = 1, r = 0.1$  and  $a = 1$ . The initial value of adaptive single parameter is selected as  $\hat{\xi}(0) = 400$ . The upper bound of approximation error is chosen as  $\varepsilon_N = 0.2$ .

**Case 1:** The proposed approach removes input saturation. The design parameters are selected as  $\lambda_{11} = 5, \lambda_{12} = 10, \lambda_{13} = 1, \lambda_{21} = 20, \lambda_{22} = 15, \lambda_{23} = 10, \mathbf{K} = \text{diag}\{150, 200, 20\}$ .

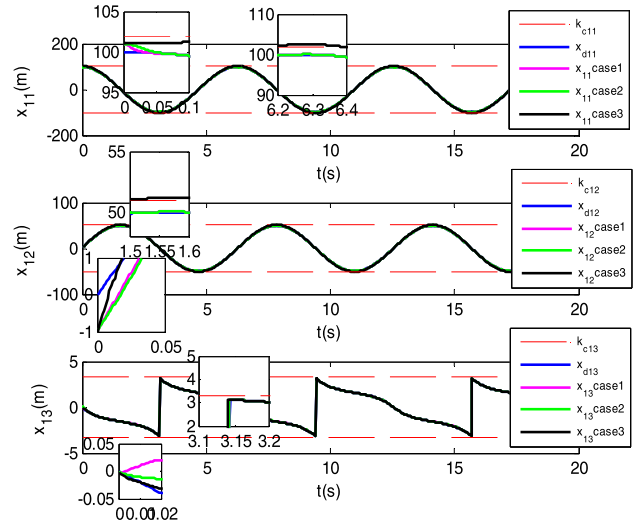


FIGURE 3. Surface vessel state  $x_{11}, x_{12}$  and  $x_{13}$  tracking desired  $x_{d11}, x_{d12}, x_{d13}$  in Case 1, 2, 3.

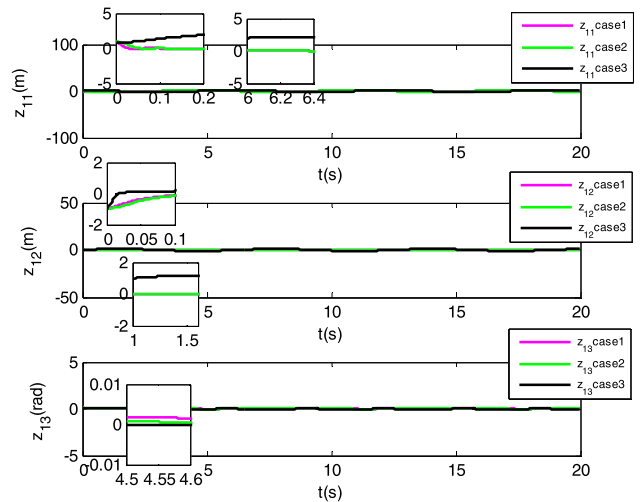


FIGURE 4. The results of the tracking errors  $z_{11}, z_{12}, z_{13}$  in Case 1, 2, 3.

**Case 2:** The proposed approach is tested. The design parameters are selected as  $\lambda_{11} = 5, \lambda_{12} = 8, \lambda_{13} = 1, \lambda_{21} = 15, \lambda_{22} = 20, \lambda_{23} = 5, \mathbf{K}_h = \text{diag}\{1, 1, 1\}, \mathbf{K}_e = \text{diag}\{10, 10, 10\}, \sigma = 1, \mathbf{e}(0) = [150, 150, 150]^T$  and  $\mathbf{K} = \text{diag}\{200, 300, 10\}$ . The range of the forces and moment is  $\tau_1 \in [-180, 180], \tau_2 \in [-370, 370]$  and  $\tau_3 \in [-90, 90]$ .

**Case 3:** A standard backstepping approach is tested without input saturation. The Lyapunov function of (41) is replaced by  $V_2 = \frac{1}{2}z_1^T z_1 + \frac{1}{2}z_2^T M z_2 + \frac{1}{2r}\tilde{\xi}^2$ . The virtual law is designed as  $\boldsymbol{\alpha}_1 = \mathbf{R}^T(-\mathbf{K}_1 z_1 + \dot{\mathbf{x}}_{d1})$ , and control law is designed as  $\boldsymbol{\tau} = -\frac{1}{2a^2}z_2 \hat{\xi} \circ (\mathbf{h} \circ \mathbf{h}) - \mathbf{K}z_2 - \mathbf{R}^T(x_2)z_1 - \bar{\eta} \text{sgn}(z_1)$ , where  $\mathbf{K}_1 = \{5, 10, 1\}$  and  $\mathbf{K} = \{150, 200, 20\}$ . The remaining parameters are the same as Case 1.

The simulation results are shown in Figs. 3-7. The surface vessel can track the reference trajectory with a high precision, and never violates the constraints. That is, the system state  $\mathbf{x}_1(t) \in \Omega_{x1}$  and  $\mathbf{x}_2(t) \in \Omega_{x2}$  in Case 1 as shown in Figs. 3 and 5. However, the proposed method in Case 1 does

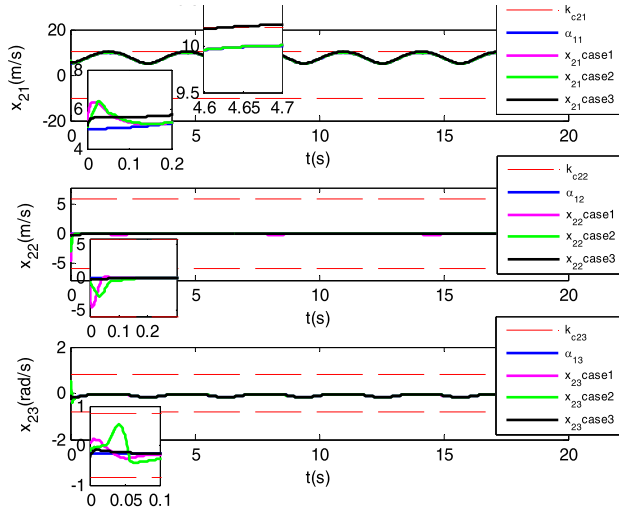


FIGURE 5. Surface vessel state  $x_{21}$ ,  $x_{22}$ ,  $x_{23}$  tracking desired  $\alpha_{11}$ ,  $\alpha_{12}$ ,  $\alpha_{13}$  in Case 1, 2, 3.

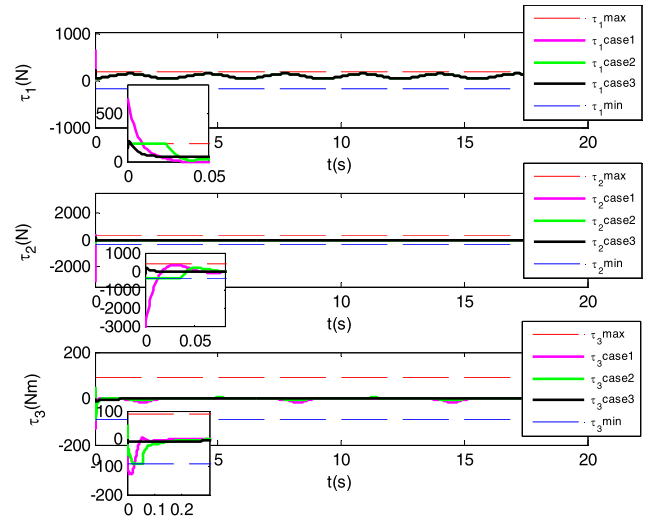


FIGURE 7. Surge control force  $\tau_1$ , sway control force  $\tau_2$ , and yaw control torque  $\tau_3$  in Case 1, 2, 3.

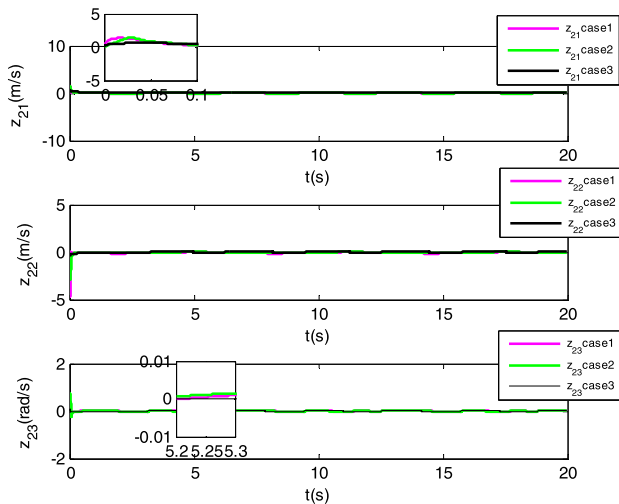


FIGURE 6. The results of the tracking errors  $z_{21}$ ,  $z_{22}$ ,  $z_{23}$  in Case 1, 2, 3.

not consider input saturation, the control signal  $\tau$  exceeds the upper and lower limits as shown in Fig. 7.

In Case 2 we consider the input saturation problem under constraints as shown in Figs. 3 and 5. Similarly, the surface vessel can also track the reference trajectory, and system state  $x_1(t)$  and  $x_2(t)$  never violates the borders of the constraints. Compared with Case 1, the auxiliary analysis system compensate for the input saturation. The control signal do not exceed the upper and lower limits as shown in Fig. 7.

In Case 1, 2 and 3, RBFNN (based on a single parameter) approach is used to compensate for nonlinear terms in the control law. In Case 1 and Case 2, the tracking errors  $z_1(t)$  and  $z_2(t)$  are all bounded, and converge to near zero as shown in Figs. 4 and 6. Tracking errors  $z_{11}$  and  $z_{12}$  in Case 3 are larger than those in Case 1 and Case 2. In addition, there is no input saturation in Case 3. From Fig. 7, it shows that the control signal  $\tau_1$  exceeds the limits. Compared with Case 3, we can conclude that our proposed control approach (with input saturation) is effective.

For Case 3, the simulation results of the standard backstepping approach without input saturation and full-state constraints as shown in Figs. 3, 5 and 7. From Figs. 3 and 5, we can see that although the surface vessel can also track the desired trajectory, the system state  $x_{11}$ ,  $x_{12}$  and  $x_{21}$  violates constraints and can not satisfy control objectives.

**Part II:** In this part, we choose the initial values of the system as  $\eta(0) = [0.5, 9.5, 0.087]^T$  and  $\nu(0) = [-0.2, 1.5, 0]^T$ , respectively. The constrains are  $k_{c1} = [8, 15, 2]^T$  and  $k_{c2} = [15, 15, 3.5]^T$ , respectively. We select the same simplified model of real environment disturbance as in [30].

The disturbance vector is set as

$$d(t) = [d_1(t), d_2(t), d_3(t)]^T = \begin{bmatrix} 1.3 + 2.0 \sin 0.02t + 1.5 \sin 0.1tN \\ -0.9 + 2.0 \sin(0.02t - \pi/6) + 1.5 \sin 0.3tN \\ -\sin(0.09t + \pi/3) - 4 \sin 0.01tNm \end{bmatrix}$$

The parameters of RBFNNs are selected as  $b_{ij} = 50$ ,  $\varpi = 0.1$ ,  $r = 0.1$ ,  $a = 1$  and  $\varepsilon_N = 0.5$ . The center  $c_{ij}$  in (31) are all  $9 \times 512$  matrices, whose elements are 1 and  $-1$ . The initial value of adaptive single parameter is selected as  $\hat{\xi}(0) = 20$ . Similarly, we still consider three cases which are the same as Case 1, Case 2 and Case 3 in Part I.

The parameters selection in Case 1 are  $\lambda_{11} = 15$ ,  $\lambda_{12} = 20$ ,  $\lambda_{13} = 2$ ,  $\lambda_{21} = 30$ ,  $\lambda_{22} = 25$ ,  $\lambda_{23} = 20$  and  $K = \text{diag}\{300, 400, 10\}$ .

The parameters in Case 2 and other settings are  $\lambda_{11} = 10$ ,  $\lambda_{12} = 30$ ,  $\lambda_{13} = 5$ ,  $\lambda_{21} = 15$ ,  $\lambda_{22} = 20$ ,  $\lambda_{23} = 20$ ,  $\sigma = 1$   $K_h = \text{diag}\{5, 5, 5\}$ ,  $K_e = \text{diag}\{20, 20, 20\}$ ,  $e(0) = [50, 50, 50]^T$   $K = \text{diag}\{350, 450, 15\}$ ,  $\tau_1 \in [-450, 450]$ ,  $\tau_2 \in [-650, 650]$  and  $\tau_3 \in [-180, 180]$ .

The parameters selection in Case 3 are  $K_1 = \{15, 20, 2\}$  and  $K = \text{diag}\{300, 400, 10\}$ . The remaining parameters are the same as Case 1.

The simulation results are shown in Figs. 8-14. From Fig. 8, it is observed that the control law in Case1, 2, 3 are all

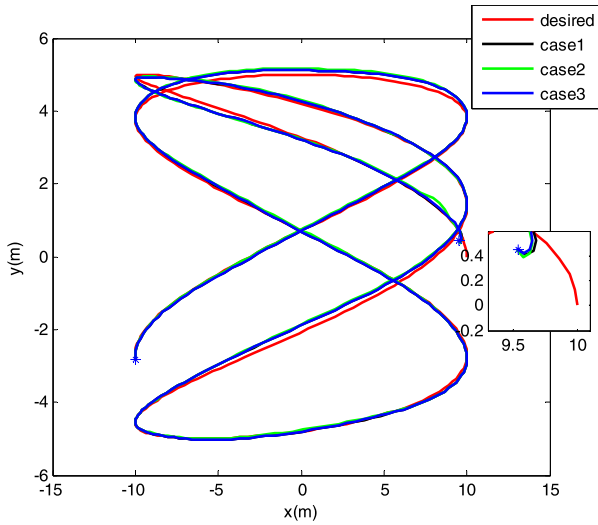


FIGURE 8. Desired and reference trajectories in xy-plane.

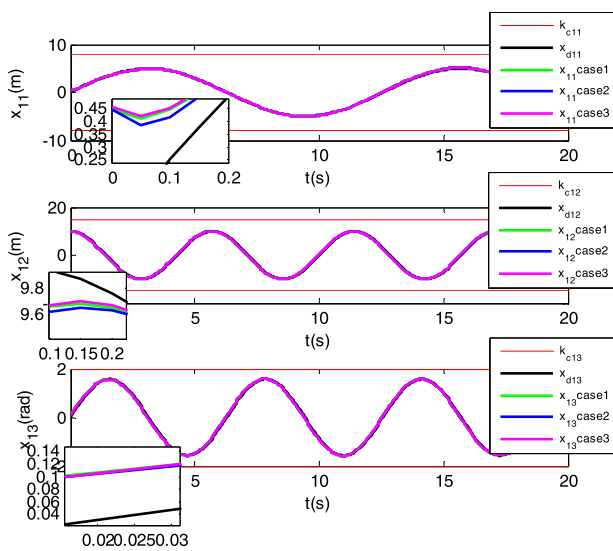


FIGURE 9. Surface vessel state  $x_{11}$ ,  $x_{12}$  and  $x_{13}$  tracking desired  $x_{d11}$ ,  $x_{d12}$ ,  $x_{d13}$  in Case 1, 2, 3.

able to control the vessel to track the reference trajectory. Furthermore, in Case 1, 2, 3, the state curves of the desired and actual positions and yaw angles are shown in Fig. 9, which shows that the actual vessel position ( $x = x_{11}$ ,  $y = x_{12}$ ) and yaw angle  $\psi = x_{13}$  can track the desired trajectory  $\eta_d = [x_d, y_d, \psi_d]^T$  with a good precision without violating the constraints. Figure 10 shows the boundedness of tracking error signals  $z_1 = [z_{11}, z_{12}, z_{13}]^T$  in three cases.

Similarly, in Case 1, 2, 3, the state curves of the desired and actual velocity including surge, sway and yaw are shown in Fig. 11, which shows that the actual vessel surge velocity  $u = x_{21}$ , sway velocity  $v = x_{22}$  and yaw velocity  $r = x_{23}$  can track the desired  $\alpha_1 = [\alpha_{11}, \alpha_{12}, \alpha_{13}]^T$  at a good precision without violating the constraints. Figure 12 shows the boundedness of tracking error signals  $z_2 = [z_{21}, z_{22}, z_{23}]^T$  in three cases.

*Remark 6:* It is worth noting that the control law designed based on the standard backstepping approach in Case 3

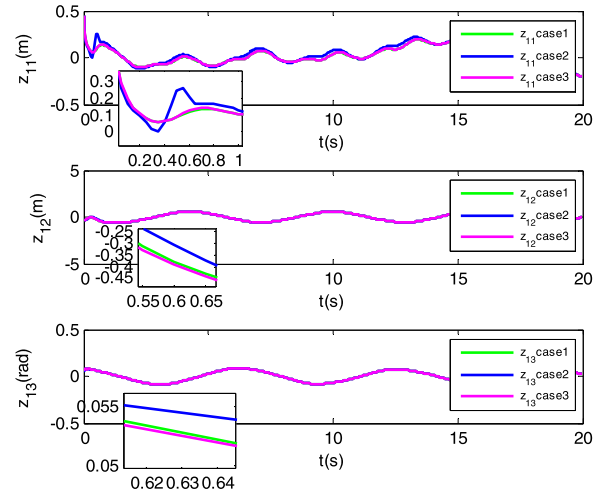


FIGURE 10. The results of the tracking errors  $z_{11}$ ,  $z_{12}$ ,  $z_{13}$  in Case 1, 2, 3.

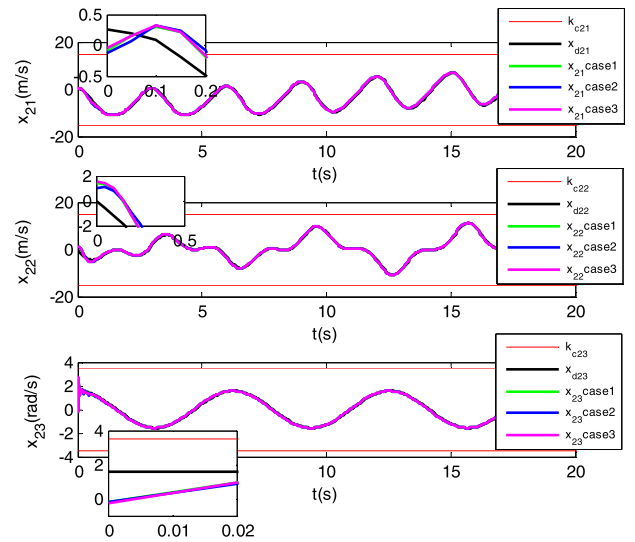


FIGURE 11. Surface vessel state  $x_{21}$ ,  $x_{22}$ ,  $x_{23}$  tracking desired  $\alpha_{11}$ ,  $\alpha_{12}$ ,  $\alpha_{13}$  in Case 1, 2, 3.

satisfies the full-state constraints through the control parameters, but does not guarantee that the vessel state satisfies the constraints in theory. In other words, the transient and steady state of the surface vessel tracking state does not satisfies the constraints theoretically.

The simulation of control law in three cases are presented in Fig. 13, which shows that the generalized control forces are reasonable. Compared with Case 1 and Case 3, the auxiliary analysis system used in Case 2 effectively handles input saturation, and the control signal does not exceed the limits.

Similarly, in Case 1, 2 and 3, RBFNN (based on a single parameter) is used to approximate the unknown nonlinear term composed of system model parameters in the control law, which is faster and more efficient than RBFNN to compensates the control law as shown in Fig. 14.

*Remark 7:* An effective neural network (NN) is selected to approximate the unknown nonlinear continuous function. Meanwhile, with the increase of the number of nodes and the dimension of approximation function of the neural network,

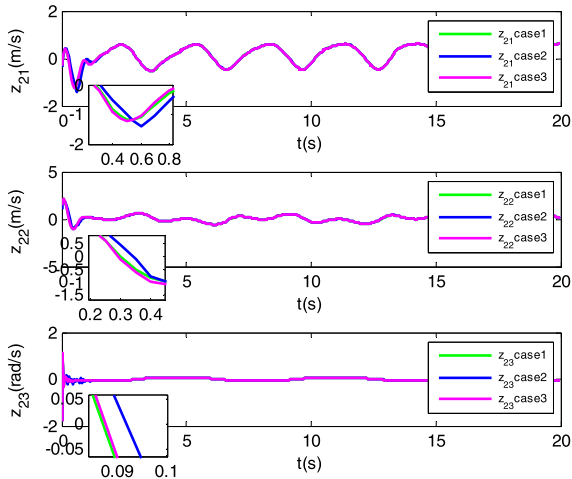


FIGURE 12. The results of the tracking errors  $z_{21}$ ,  $z_{22}$ ,  $z_{23}$  in Case 1, 2, 3.

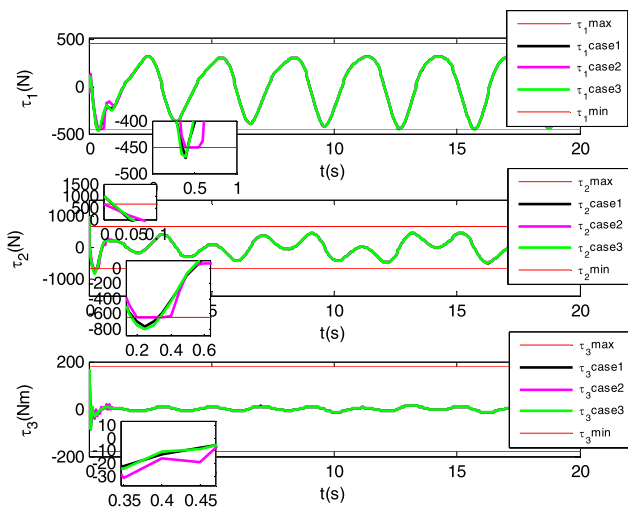


FIGURE 13. Surge control force  $\tau_1$ , sway control force  $\tau_2$ , and yaw control torque  $\tau_3$  in Case 1, 2, 3.

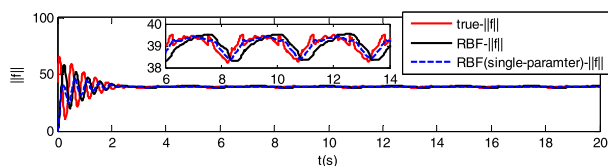


FIGURE 14. Comparison of simulation results of nonlinear continuous  $\|f\|$  approximation.

it is necessary to adjust the weights in the NN, which requires a lot of calculation, requires longer running time to generate control signals, and also brings difficulties to practical application. According to the inherent property of the square of the NN’s base vector, the ideal weight matrix estimation of the neural network is converted into a single parameter estimation, which accelerates the solution of the adaptive law, reduces the computational complexity and approximates the unknown nonlinear continuous function faster and better.

*Remark 8:* Theorem 1 shows that the signals of the closed-loop system remain bounded under the given constraint sets by selecting the desired trajectory and setting the initial values in the compact set  $\Omega_{x1}$  and  $\Omega_{x2}$ . Further, it can be concluded

that the error signals  $z_1$ ,  $z_2$  and  $\tilde{\xi}$  uniformly ultimately bounded in the compact set dependent on constants  $C$  and  $\rho$ . The size of the final convergence set of error signals  $\lim_{t \rightarrow \infty} \|z_1\| \leq \sqrt{\frac{2C}{\rho}}$ ,  $\lim_{t \rightarrow \infty} \|z_2\| \leq \sqrt{\frac{2C}{\rho}} \cap \lim_{t \rightarrow \infty} \|z_2\| \leq \sqrt{\frac{2C}{\lambda_{\max}(M)\rho}}$  and  $\lim_{t \rightarrow \infty} |\tilde{\xi}| \leq \sqrt{\frac{2rC}{\rho}}$  can be reduced by decreasing constant  $C$  and increasing constant  $\rho$ . In order to reduce  $C$ , it is necessary to select smaller parameters  $\sigma$ ,  $\delta$ ,  $\varpi$ ,  $a$  and  $K_h$ . In order to increase  $\rho$ , it is necessary to select larger parameters  $\lambda_{1i}$ ,  $\lambda_{2i}$ ,  $\varpi r$ ,  $K$  and  $K_e - \frac{1}{2}K_h^T K_h$ ,  $i = 1, 2, 3$ , and increasing constant is helpful for a fast convergence. However, if  $\varpi r$  is too small, it may result in an increase in the adaptive parameter estimate  $\tilde{\xi}$  and a reduced robustness of the closed-loop system. If we choose too large  $\lambda_{1i}$ ,  $\lambda_{2i}$  to improve the robustness and get better tracking performance, then too large  $\lambda_{1i}$  will cause the upper bound function  $A_{1(i-1)}$  to be large, which may lead to the state constraint  $|\alpha_{1i}| < k_{c2i}$  to be satisfied. In addition, too large  $\lambda_{1i}$  and  $\lambda_{2i}$  may lead to increased control input and unmodeled dynamics. Then, an increase in control input may cause the excessive difference between the designed input signal  $\tau_c$  and the saturation output signal  $\tau$ , that is, if the saturation limits  $\tau_{imax}$  and  $\tau_{imin}$  are too small, there may be no control parameters to satisfy both state constraints and input saturation. We make  $\kappa_i > 0$  represent the maximum feasible difference between the preset actual control input signal  $\tau_{ci}$  and the saturation output signal  $\tau_i$  to ensure the controllability of surface vessels (1) under the input saturation (3). Furthermore, the controllability condition under input saturation is described as  $\delta_i = |\tau_i - \tau_{ci}| < \kappa_i$ , which is used as a condition for the design of control systems. In practice, the value of  $\kappa_i$  needs to be set according to the system actuator parameters and requirements.

To maximize the tracking performance and balance the parameters of feasibility. We introduce the relevant parameter adjustment approach for Cases 1 and 2. The feasibility conditions of the parameters are  $|x_{d1}| \leq A_{0(i-1)} < k_{c1i}$ ,  $\max |\alpha_{1i}| = A_{1(i-1)}(\lambda_{1i}) < k_{c2i}$ , ( $\kappa_i > \delta_i(\lambda_{1i}, \lambda_{2i})$ ). We convert the detection approach of feasibility solution condition into a nonlinear constrained optimization problem. The optimal control parameters  $\lambda_{1i}$ ,  $\lambda_{2i}$  are obtained by detecting the feasibility solution conditions under given state constraints  $k_{c1i}$ ,  $k_{c2i}$  and initial values, so that the output tracking performance can be maximized when full-state constraints are satisfied with input saturation.

## V. CONCLUSION

In this paper, the backstepping technique has been augmented with a iBLF, RBFNNs, sliding mode and the dynamic auxiliary analysis system to realize trajectory tracking for a fully actuated surface vessel subjected to full-state constraints, input saturation and system uncertainties.

First, a control system with constraints is constructed by constructing iBLF instead of the log-type BLF, which can effectively deal with the system constraints directly and prevent the system state from violating the constraints.

Second, the RBFNNs approximation is introduced to approximate the unknown parameters of the system to compensate for the control law, and the ideal weight matrix estimation of the neural network is converted into a single parameter for adaptive adjustment. In this way, the number of adaptive parameters is reduced, and so is the calculation complexity. Therefore, the real-time performance is improved. In addition, a sliding mode is introduced to overcome the approximation error term.

Third, considering the physical constraints of actuators, a dynamic auxiliary analysis system is employed to deal with input saturation.

Finally, All signals in the closed-loop system are proved to be bounded using Lyapunov theory. Simulation results verify proposed control approach. In future, input time-delay should be discussed for trajectory tracking control of surface vessels with full-state constraints and input saturation.

## REFERENCES

- [1] M. Fu, M. Li, and W. Xie, "Finite-time trajectory tracking fault-tolerant control for surface vessel based on time-varying sliding mode," *IEEE Access*, vol. 6, pp. 2425–2433, 2017.
- [2] N. Wang, C. Qian, J.-C. Sun, and Y.-C. Liu, "Adaptive robust finite-time trajectory tracking control of fully actuated marine surface vehicles," *IEEE Trans. Control Syst. Technol.*, vol. 24, no. 4, pp. 1454–1462, Jul. 2016.
- [3] N. Wang and M. J. Er, "Direct adaptive fuzzy tracking control of marine vehicles with fully unknown parametric dynamics and uncertainties," *IEEE Trans. Control Syst. Technol.*, vol. 24, no. 5, pp. 1845–1852, Sep. 2016.
- [4] H. Ashrafiuon, K. R. Muske, L. C. McNinch, and R. A. Soltan, "Sliding-mode tracking control of surface vessels," *IEEE Trans. Ind. Electron.*, vol. 55, no. 11, pp. 4004–4012, Nov. 2008.
- [5] J. F. Jiao and G. Wang, "Event triggered trajectory tracking control approach for fully actuated surface vessel," *Neurocomputing*, vol. 182, pp. 267–273, Mar. 2016.
- [6] J. Guldner and V. I. Utkin, "Sliding mode control for gradient tracking and robot navigation using artificial potential fields," *IEEE Trans. Robot. Automat.*, vol. 11, no. 2, pp. 247–254, Apr. 1995.
- [7] T. Zhang, Y. Zhu, and J. Song, "Real-time motion planning for mobile robots by means of artificial potential field method in unknown environment," *Ind. Robot, Int. J.*, vol. 37, no. 4, pp. 384–400, 2010.
- [8] C. Liu, J. Sun, and Z. Zou, "Integrated line of sight and model predictive control for path following and roll motion control using rudder," *J. Ship Res.*, vol. 59, no. 2, pp. 99–112, Jun. 2015.
- [9] D. Q. Mayne, J. B. Rawlings, C. V. Rao, and P. O. M. Scokaert, "Constrained model predictive control: Stability and optimality," *Automatica*, vol. 36, no. 6, pp. 789–814, 2000.
- [10] S. Oлару, J. A. De Doná, M. M. Seron, and F. Stoican, "Positive invariant sets for fault tolerant multisensor control schemes," *Int. J. Control*, vol. 83, no. 12, pp. 2622–2640, Dec. 2010.
- [11] S. V. Rakovic, E. C. Kerrigan, K. I. Kouramas, and D. Q. Mayne, "Invariant approximations of the minimal robust positively invariant set," *IEEE Trans. Autom. Control*, vol. 50, no. 3, pp. 406–410, Mar. 2005.
- [12] B. Ren, S. S. Ge, K. P. Tee, and T. H. Lee, "Adaptive control for parametric output feedback systems with output constraint," in *Proc. 48th IEEE Conf. Decis. Control (CDC) Held Jointly 28th Chin. Control Conf.*, Dec. 2009, pp. 6650–6655.
- [13] K. P. Tee and S. S. Ge, "Control of nonlinear systems with partial state constraints using a barrier Lyapunov function," *Int. J. Control*, vol. 84, no. 12, pp. 2008–2023, 2011.
- [14] K. P. Tee, S. S. Ge, H. Li, and B. Ren, "Control of nonlinear systems with time-varying output constraints," *Automatica*, vol. 47, no. 11, pp. 2511–2516, Nov. 2011.
- [15] B. Ren, S. S. Ge, K. P. Tee, and T. H. Lee, "Adaptive neural control for output feedback nonlinear systems using a barrier Lyapunov function," *IEEE Trans. Neural Netw.*, vol. 21, no. 8, pp. 1339–1345, Aug. 2010.
- [16] Z.-L. Tang, S. S. Ge, K. P. Tee, and W. He, "Adaptive neural control for an uncertain robotic manipulator with joint space constraints," *Int. J. Control*, vol. 89, no. 7, pp. 1428–1446, Feb. 2016.
- [17] Z.-L. Tang, S. S. Ge, K. P. Tee, and W. He, "Robust adaptive neural tracking control for a class of perturbed uncertain nonlinear systems with state constraints," *IEEE Trans. Syst., Man, Cybern. Syst.*, vol. 46, no. 12, pp. 1618–1629, Dec. 2016.
- [18] D.-J. Li, J. Li, and S. Li, "Adaptive control of nonlinear systems with full state constraints using integral barrier Lyapunov functionals," *Neurocomputing*, vol. 186, pp. 90–96, Apr. 2016.
- [19] Z. Zhao, W. He, and S. S. Ge, "Adaptive neural network control of a fully actuated marine surface vessel with multiple output constraints," *IEEE Trans. Control Syst. Technol.*, vol. 22, no. 4, pp. 1536–1543, Jul. 2014.
- [20] Z. Yin, W. He, and C. Yang, "Tracking control of a surface vessel with full-state constraints," *Int. J. Syst. Sci.*, vol. 48, no. 3, pp. 535–546, Aug. 2017.
- [21] C. Wen, J. Zhou, Z. Liu, and H. Su, "Robust adaptive control of uncertain nonlinear systems in the presence of input saturation and external disturbance," *IEEE Trans. Autom. Control*, vol. 56, no. 7, pp. 1672–1678, Jul. 2011.
- [22] H. Wang, B. Chen, X. Liu, K. Liu, and C. Lin, "Robust adaptive fuzzy tracking control for pure-feedback stochastic nonlinear systems with input constraints," *IEEE Trans. Cybern.*, vol. 43, no. 6, pp. 2093–2104, Dec. 2013.
- [23] A. Veksler, T. A. Johansen, F. Borrelli, and B. Realfsen, "Dynamic positioning with model predictive control," *IEEE Trans. Control Syst. Technol.*, vol. 24, no. 4, pp. 1340–1353, Jul. 2016.
- [24] T. Perez and A. Donaire, "Constrained control design for dynamic positioning of marine vehicles with control allocation," *Model. Identificat. Control*, vol. 30, no. 2, pp. 57–70, 2009.
- [25] M. Chen, S. S. Ge, and B. V. E. How, "Robust adaptive neural network control for a class of uncertain MIMO nonlinear systems with input nonlinearities," *IEEE Trans. Neural Netw.*, vol. 21, no. 5, pp. 796–812, May 2010.
- [26] J. Du, X. Hu, M. Krstić, and Y. Sun, "Robust dynamic positioning of ships with disturbances under input saturation," *Automatica*, vol. 73, pp. 207–214, Nov. 2016.
- [27] T. I. Fossen and A. Grovlen, "Nonlinear output feedback control of dynamically positioned ships using vectorial observer backstepping," *IEEE Trans. Control Syst. Technol.*, vol. 6, no. 1, pp. 121–128, Jan. 1998.
- [28] W. He, S. Zhang, and S. S. Ge, "Boundary control of a flexible riser with the application to marine installation," *IEEE Trans. Ind. Electron.*, vol. 60, no. 12, pp. 5802–5810, Dec. 2013.
- [29] W. He, B. V. E. How, S. S. Ge, and Y. S. Choo, "Boundary control of a flexible marine riser with vessel dynamics," in *Proc. Amer. Control Conf.*, Baltimore, MD, USA, Jun./Jul. 2010, pp. 1532–1537.
- [30] Y. Yang, J. Du, H. Liu, C. Guo, and A. Abraham, "A trajectory tracking robust controller of surface vessels with disturbance uncertainties," *IEEE Trans. Control Syst. Technol.*, vol. 22, no. 4, pp. 1511–1518, Jul. 2014.
- [31] J. Ghommam, F. Minif, A. Benali, and G. Poisson, "Observer design for Euler Lagrange systems: Application to path following control of an underactuated surface vessel," in *Proc. IEEE/RSJ Int. Conf. Intell. Robots Syst.*, San Diego, CA, USA, Oct./Nov. 2007, pp. 2883–2888.
- [32] R. Yu, Q. Zhu, G. Xia, and Z. Liu, "Sliding mode tracking control of an underactuated surface vessel," *IET Control Theory Appl.*, vol. 6, no. 3, pp. 461–466, 2012.
- [33] Y. Zhang, P.-Y. Peng, and Z.-P. Jiang, "Stable neural controller design for Unknown nonlinear systems using backstepping," *IEEE Trans. Neural Netw.*, vol. 11, no. 6, pp. 1347–1360, Nov. 2000.
- [34] T. Zhang, S. S. Ge, and C. C. Hang, "Adaptive neural network control for strict-feedback nonlinear systems using backstepping design," *Automatica*, vol. 36, no. 12, pp. 1835–1846, 2000.
- [35] C. Kwan and F. L. Lewis, "Robust backstepping control of nonlinear systems using neural networks," *IEEE Trans. Syst., Man, Cybern. A, Syst. Humans*, vol. 30, no. 6, pp. 753–766, Nov. 2000.
- [36] S. S. Ge and C. Wang, "Direct adaptive neural network control of a class of nonlinear systems," *IEEE Trans. Neural Netw.*, vol. 13, no. 1, pp. 214–221, Jan. 2002.
- [37] H. Zhang and G. Zhang, "Adaptive backstepping sliding mode control for nonlinear systems with input saturation," *Trans. Tianjin Univ.*, vol. 18, no. 1, pp. 46–51, Feb. 2012.
- [38] B. Miao, T. Li, W. Luo, and X. Gao, "NN based adaptive dynamic surface control for fully actuated AUV," *Nonlinear Dyn.*, vol. 84, no. 2, pp. 1079–1091, 2013.

[39] L. Ma, K. Schilling, and C. Schmid, "Adaptive backstepping sliding mode control with Gaussian networks for a class of nonlinear systems with mismatched uncertainties," in *Proc. 44th IEEE Conf. Decis. Control*, Seville, Spain, Dec. 2015, pp. 5504–5509.

[40] K. P. Tee, S. S. Ge, and E. H. Tay, "Barrier Lyapunov functions for the control of output-constrained nonlinear systems," *Automatica*, vol. 45, no. 4, pp. 918–927, Apr. 2009.

[41] S. S. Ge, T. H. Lee, and C. J. Harris, *Adaptive Neural Network Control of Robotic Manipulators*. Singapore: World Scientific, 1998.

[42] Z. Liu, C. Chen, Y. Zhang, and C. L. P. Chen, "Adaptive neural control for dual-arm coordination of humanoid robot with unknown nonlinearities in output mechanism," *IEEE Trans. Cybern.*, vol. 45, no. 3, pp. 507–518, Mar. 2015.

[43] D.-P. Li and D.-J. Li, "Adaptive neural tracking control for an uncertain state constrained robotic manipulator with unknown time-varying delays," *IEEE Trans. Syst., Man, Cybern. Syst.*, vol. 48, no. 12, pp. 2219–2228, Dec. 2018.

[44] S. S. Ge, C. C. Hang, T. H. Lee, and T. Zhang, *Stable Adaptive Neural Network Control*. Norwell, MA, USA: Kluwer, 2001.

[45] R. Skjetne, T. I. Fossen, and P. V. Kokotović, "Adaptive maneuvering, with experiments, for a model ship in a marine control laboratory," *Automatica*, vol. 41, no. 2, pp. 289–298, Feb. 2005.

[46] T. I. Fossen, *Handbook of Marine Craft Hydrodynamics and Motion Control*. New York, NY, USA: Wiley, 2011.



**XIYUN JIANG** received the M.E. degree from the Heilongjiang Institute of Science and Technology, Harbin, China, in 2015. He is currently pursuing the Ph.D. degree in control science and engineering with Harbin Engineering University, Harbin. His current research interests include sliding mode control, neural network control, and surface vessel motion control.



**WENCHAO SHE** received the B.E. degree in electrical engineering and its automation from Harbin Engineering University, China, in 2017, where he is currently pursuing the M.E. degree in control science and engineering. His current research interests include guidance and collision avoidance control for marine surface vessels, and non-linear motion control.



**YUANHUI WANG** received the B.S., M.S., and Ph.D. degrees from Harbin Engineering University, Harbin China, where she is currently an Associate Professor with the College of Automation. Her research interests include guidance, navigation and control of marine crafts, ship dynamic positioning, ship dynamics and motion control, robot path planning, and signal processing.



**FUGUANG DING** received the M.S. degree from Harbin Engineering University, Harbin, China, where he is currently a Professor with the College of Automation. His research interests include ship motion control, ship dynamic positioning, hardware-in-loop simulation technique, and embedded system application.

...